Environmental Science
Processes & Impacts

PAPER

View Article Online
View Journal | View Issue

Cite this: *Environ. Sci.: Processes Impacts*, 2019, **21**, 528

Seasonal variation in aerosol composition and concentration upon transport from the outdoor to indoor environment†

Anita M. Avery, [ac] Michael S. Waring [a] and Peter F. DeCarlo *[ab]

Outdoor-originated aerosols are an important component impacting indoor air quality. Since outdoor aerosols vary over short (diurnal) and long (seasonal) timescales, we examined how the variation in outdoor aerosol concentration and composition impact indoor aerosol. Measurements of both indoor and outdoor aerosol composition in real time in an urban classroom in winter and summer seasons were performed using an aerosol mass spectrometer (AMS), aethalometer, and a suite of gas phase instruments. Factor analysis of the organic aerosol components identified three factors in common between seasons, including hydrocarbon-like, cooking, and oxidized organic aerosol (HOA, COA, and OOA). Since sulfate is non-volatile, we report a sulfate-normalized indoor–outdoor ratio $(I/O)_{i/SO_4}$ for measured aerosol *i* components, allowing us to estimate aerosol component-based effects of seasonal and other variations in ventilation and HVAC operation, indoor emission sources, and chemically-based loss processes between outdoor and indoor environments. These chemical loss processes are interpreted in terms of changes in temperature and relative humidity (RH) between environments, which fluctuate on a daily and seasonal basis. The degree to which any effect is observed depends on the particular outdoor aerosol population and the magnitude of temperature or RH change. In wintertime, when aerosols were warmed upon transport indoors and loss of volatile components is favored, median $(I/O)_{i/SO_4}$ values for nitrate, total organics, HOA, and BC were smaller (0.35, 1.00, 1.24, and 1.18, respectively) than summertime values (0.75, 1.17, 1.96, and 1.80). For COA and OOA, however, $(I/O)_{i/SO_4}$ values were higher in the winter than in summer. Calculated aerosol liquid water (ALW), which is a function of temperature and RH and the relative contribution of hygroscopic components, varied significantly by season. Summertime ALW indoors provides a medium for aqueous processing, which is necessary for some hydrophilic gas phase reaction products that are important to indoor air quality and occupant exposure. This work describes the linkages between seasonal variability in aerosol composition outdoors and the subsequent chemically-specific variation observed when that aerosol is brought indoors.

Received 15th October 2018
Accepted 23rd January 2019

DOI: 10.1039/c8em00471d

rsc.li/espi

Environmental significance

Outdoor aerosols are regulated by governments worldwide to reduce exposure and protect human health. In the developed world, however, people spend the vast majority of their time indoors. Consequently, exposure to outdoor aerosols predominantly occurs in the indoor environment. This study aims to quantify the impact of temperature and relative humidity gradients on the composition and transport of aerosol particles from the outdoor to the indoor environment in both the summer and winter seasons when temperature gradients between indoors and outdoors are reversed. The results presented here can be used to inform models of indoor air quality and provide insight into how outdoor aerosol is modified when transported indoors.

1. Introduction

1.1 Seasonal-dependence of outdoor-originated aerosol

High concentrations of ambient aerosols have been linked to adverse respiratory and cardiovascular conditions.[1] Humans spend most of their time indoors.[2] However, for practical and legislative reasons, we monitor and regulate outdoor air quality with improving human health as one of the aims. Seasonal-dependent fluctuations in outdoor aerosol concentration and

[a]*Department of Civil, Architectural, and Environmental Engineering, Drexel University, USA. E-mail: pfd33@drexel.edu*

[b]*Department of Chemistry, Drexel University, USA*

[c]*Now at Center for Aerosol and Cloud Chemistry, Aerodyne Research, Inc, USA*

† Electronic supplementary information (ESI) available. See DOI: 10.1039/c8em00471d

composition, and by extension, exposure to them is dependent on meteorological conditions (*e.g.* natural boundary layer height variability), seasonal processes (photochemical variation with season), and variability in source emissions (*e.g.* heating-specific emissions in winter). However, long-term in-depth characterization of outdoor aerosols is difficult because most field work is time constrained with typical sampling durations on the order of one month. The IMPROVE network[3] has investigated chemical speciation *via* integrated filter samples at 110 locations, some operating since 1985, but are limited to rural areas and predominantly in National Parks and Wilderness Areas in the United States. This limits application to exposure between the indoor and outdoor environments. Other monitoring networks including the EPA air quality monitoring stations provide more local level data, but are similarly limited by time integrated filters. Recent instrument developments like the Aerosol Chemical Speciation Monitor (ACSM),[4] which can sample independently and continuously for weeks to months, has made long-term inter-seasonal and inter-annual measurements more common in urban areas.[5,6]

More than a decade of aerosol mass spectrometer (AMS) measurements, providing minute-to-hour integrated real-time submicron aerosol composition,[7,8] across the world have resulted in several chemically-specific inter-seasonal analyses of mega cities.[9–13] Despite continental, latitudinal, annual, and intra-city differences, trends in aerosol composition and chemical processing have emerged, contributing greatly to our understanding of tropospheric outdoor aerosols. By bringing the AMS measurement methods to the indoor environment, we provide new insights to aerosol exposure indoors, utilizing the knowledge gained from outdoor sampling with the AMS.[14,15] This work provides a direct comparative analysis for outdoor aerosol species transported to the indoor environment and the influence of sources and processes occurring in the indoor environment.

1.2 Indoor–outdoor ratio

Chemical species from the outdoors make their way indoors *via* several important mechanisms (*e.g.* ventilation, infiltration),[16,17] and emissions in each environment and processing between them are important parameters of exposure. For environments with minimal indoor sources, the influence of outdoor aerosol on the indoor environment can be succinctly described with the indoor/outdoor (I/O) ratio:[18] the concentration of indoor aerosol normalized by that of outdoor. For environments with indoor sources including cooking,[19] cleaning,[20,21] smoking,[22] or other emission sources, the I/O ratio can exceed unity, but trends of the I/O ratio over time provide insights into the sources of aerosols to the indoor environment. The I/O ratio has been widely used to describe penetration and infiltration across building types, environmental conditions, and outdoor emission types,[23] but without the ability to compare directly across these important operating conditions, and has been used with limited discussion as to the diverse characteristics of the outdoor-originated aerosols.

Johnson *et al.*[14] described a sulfate-normalized I/O ratio as the I/O ratio of any aerosol chemical component i divided by the I/O ratio of non-volatile sulfate, $(I/O)_i/(I/O)_{SO_4} = (I/O)_{i/SO_4}$, as a first order parameter to normalize for mechanical losses (*e.g.* deposition and filtration) and demonstrate the impact of additional processes on the indoor aerosol population. These additional processes include indoor emissions as well as gains or losses due to physiochemical transformation. Implicitly, the $(I/O)_{i/SO_4}$ assumes an internally mixed aerosol population or similar mechanical loss rates for externally mixed populations. Externally mixed aerosol populations that differ in size and composition complicate the use of $(I/O)_{i/SO_4}$, but trends and interpretations are still useful for understanding outdoor-to-indoor transport. Use of the $(I/O)_{i/SO_4}$ creates a basis for comparison across seasons when building ventilation differs, and provides a standardization for other regions, climates, and building operation.

1.3 Factors affecting chemical transformation: temperature, humidity, liquid water, and hygroscopic components

In addition to mechanical loss processes (*e.g.* filtration and deposition) affecting the I/O ratio, chemical transformation of aerosol upon transport from outdoors to indoors is governed by chemical-specific physiochemical properties, such as volatility. For a mechanically ventilated building, at positive temperature (T) gradients (in>out, as during midlatitude winter), the heating, ventilation, and air conditioning (HVAC) systems operating to heat outdoor air can drive semi-volatile components from the condensed phase to the gas phase and decrease the $(I/O)_{i/SO_4}$; at negative gradients (in < out, as during midlatitude summer), condensation of semi-volatile species from the gas phase to the particle phase can increase the $(I/O)_{i/SO_4}$. The positive T gradient scenario has been studied extensively outdoors using a thermodenuder coupled with an AMS;[24] however, the T gradients in these studies are often much greater than for outdoor-to-indoor environments and lack high T resolution in temperature at low ΔT. Thermodenuder work has examined some of the complexity of organic aerosol (OA) from various sources[25] or positive matrix factorization (PMF) result types.[26] Temperature gradients between indoors and outdoors on organics using the volatility basis set (VBS)[27] on relationship of indoor, outdoor and personal air (RIOPA) study data[28,29] highlighted the geo-specific relationship between outdoor aerosol volatility and indoor aerosol observations. However, the negative T gradient case (in < out, summer) has not been experimentally investigated.

While relative humidity (RH) and T are linked, the role of humidity in contributing to aerosol liquid water (ALW) uptake from hygroscopic components and subsequent re-partitioning of water soluble aerosol components with the gas phase is an important consideration in I/O ratios.[30] ALW mass globally is approximately twice that of dry aerosol,[31] indicating the ubiquitous availability of an aqueous phase for processing of both organics and inorganics,[32] and making organic aerosol dependent on temperature, humidity,[33,34] and inorganic hygroscopic components.[35] Recent field studies, especially the southern oxidant and aerosol study (SOAS),[36] have highlighted the importance of humidity and aqueous-phase processing in high-humidity environments. Long-term measurements in Beijing also showed effects seasonal-dependence of aqueous processing with humidity across oxidized PMF factors.[37]

The impact of hygroscopic growth or contraction of aerosols, dependent on chemical composition and changes in humidity across a building envelope can be analogized to hygroscopicity-tandem differential mobility analyzer (HTDMA) work, which has explored the expansion of aerosol size distribution with humidification, dependent on aerosol size, hygroscopic components, and humidity.[38–41] Further combination of analytical methods in a volatility-hygroscopicity tandem DMA (VH-TDMA)[42] have shown the hygroscopicity of volatile compounds to be high, in agreement with growth factor measurements and Zdanovskii, Stokes, and Robinson (ZSR) predictions. Growth factor calculations based on hygroscopic components and humidity link these properties with ALW and size distribution outcomes. In the indoor environment, all of these properties are expressed in their $(I/O)_{i/SO_4}$, dependent on the environmental differences and processing between environments.

2. Methods

2.1 Sampling methods

Real-time, near simultaneous measurements with the AMS and other instrumentation were taken on outdoor air and the indoor air in a classroom. Sampling took place in winter (Jan 31-Mar 2) and summer (July 13-Aug 13) 2016, at Drexel University in Philadelphia. Outdoor measurements sampled air including emissions from regional and local sources including the nearby I-76 freeway, the major transportation hub of 30th Street Station, and Center City Philadelphia. Nearby, a row of food trucks served the university on weekdays (7 AM–6 PM) with limited service until lunch on Saturday and no service on Sunday. The outdoor inlet was a dedicated inlet from the roof directly above the laboratory, next to the air intake for the HVAC zone serving the classroom where indoor air was sampled.

The classroom was 148 m^3, with tiled floors and painted cinder block walls, a chalkboard and mobile desk seating for about 25 students. There were doors on each of two adjacent walls, but one door led to another recessed room, so no direct air flow currents between the two doors were expected. The adjacent hallways were not mechanically ventilated. The room was occupied regularly for classes only during the winter season, but the number of occupants and occupant activities were not recorded. The human contribution to the indoor aerosol composition during the wintertime measurements will be discussed in detail in a future publication. The HVAC zone included adjacent faculty and student offices but no other classrooms. Sampling for each inlet was controlled by a custom valve-switching device to alternate sampling for all instruments between indoor and outdoor inlets every 4 minutes; a bypass line was utilized to ensure continuous flow at a constant rate in each inlet. Sample air was dried to below 30% RH using a Nafion Dryer (MD-700 series, Perma Pure Inc.) prior to measurement by the aerosol instrumentation.

2.2 Instrumentation

2.2.1 Soot-particle aerosol mass spectrometer (SP-AMS). The SP-AMS (Aerodyne, Inc.) used here was operated with the laser off as a high resolution time of flight (HR-ToF) AMS.[7] The AMS measured bulk and size-resolved chemical composition of non-refractory, submicron particles including organics, nitrate, sulfate, ammonium, and chloride. Data was processed using standard AMS software packages including high resolution analysis. A relative ionization efficiency of 1.4 was assumed for all organic species. A collection efficiency of 0.5 was applied as less than 8% of the winter outdoor data, and none of the indoor winter or either environment in summer met the criteria for a higher efficiency.[43] We discussed whether to apply this and are concerned that modifying the outdoor CE, but not the indoor CE may potentially introduce artifacts in the data as well. Chloride was used in the ALW calculations, but is otherwise excluded from analysis here. Ammonium was also excluded from I/O analysis since it is a function of sulfate and nitrate, and trends in its I/O ratio are due to variations in sulfate and nitrate. Predicted *versus* measured ammonium analysis, describing the aerosol acid/base neutralization state,[44] can be found in Fig. S1.† This analysis predicts the required ammonium concentration to fully neutralize the measured sulfate, nitrate, and chloride, and compares it to the measured ammonium by the AMS. CO_2 measured by the Picarro CRDS (described below) was used for mass spectra correction at m/z 44 in the fragmentation table.[45] Elemental ratios of C/H/O/N PMF factors were calculated from high resolution mass spectra.[46,47]

2.2.2 Aethalometer. The AE-33 (Magee Scientific) aethalometer[48] measured light absorption at seven wavelengths. However, only one wavelength (880 nm) was used for this analysis. Mass absorption coefficients and other calibrations, including automatic loading artifact correction, were provided by the manufacturer.

2.2.3 Picarro CRDS gas analyzer. The G2401 analyzer for CO_2, CO, CH_4, H_2O (Picarro, Inc.) used cavity ringdown spectroscopy (CRDS) to measure given gases at 0.25 Hz. It was calibrated with a calibration tank of CO_2, CO, and CH_4, was used to calibrate the instrument at 3 dilution levels each week of operation.

2.2.4 Other measurements. Indoor T and RH were measured with an Elgato Eve indoor sensor system. A Vaisala Automatic Weather Station 310 (AWS310) was located outdoors on Drexel campus for outdoor meteorological data, including T and RH, wind speed (WS), wind direction (WD), pressure (P), solar radiation, and precipitation.

2.3 Lag time and air exchange rates

Sulfate measurements were used to determine and time-shift for the time delay (or "lag") for the changes in outdoor-originated aerosols to be reflected in the indoor aerosol concentration. This shift value for each dataset captured differences in building air flows in different seasons. This time was determined with a time-shifting regression analysis, which has previously been described in detail.[14] Briefly, the peak correlation between outdoor and indoor sulfate concentration across several inlet cycles was calculated for all continuous 24 hour segments for each dataset. The aggregate of these peak correlation values resulted in a distribution of shift values, the

peak of which was chosen as the single lag value for the entire dataset. All aerosol I/O ratios presented here use the lag-time correction. These were different between seasons, with indoor data reflecting a 29 minute lag for winter and 37 minute lag for summer. However, the effect of this analysis on the ratios described here was minimal, as shown in Table S1.†

Of note, the aerosol lag shift time in this room with ventilation and recirculation air exchange, and subject to filtration, is distinct from air exchange rate as measured by gas phase species. The ventilation rate is defined as the rate of exchange of indoor air with outdoor air, and is distinct from the room air exchange rate (AER) which includes recirculation from other rooms within the HVAC zone, in addition to the ventilation rate. The ventilation rate was calculated from the discretized solution of a simple CH_4 model using measured indoor and outdoor concentrations, as described in eqn (1):[18]

$$\frac{dC}{dt} = \lambda C_{out} - \lambda C \quad (1)$$

where the change in time (t) of indoor concentration (C) of CH_4 is described by the air exchange rate (λ) and the outdoor concentration (C_{out}).

The room AER was calculated from the average decay of CO_2 after releases (performed multiple times per season). In each season, the calculated lag time (converted to an air exchange rate) fell between ventilation rate and room AER. In winter, the ventilation and room AERs were 0.39 and 3.5 h^{-1} and in summer, 0.17 and 4.1 h^{-1}. Seasonal differences are reflective of operational changes in the HVAC system.

2.4 Organic and inorganic nitrate aerosol

Nitrate has been separated into contributions from inorganic nitrate (iNO_3) and organic-nitrate (oNO_3) based on the ratio of high resolution NO_2^+ to NO^+ ions.[49,50] Measured nitrate fragments NO^+, and NO_2^+ can originate from organic (*i.e.* $RONO_2$) or inorganic (*i.e.* NH_4NO_3) molecules. The ratio R of NO_2^+ to NO^+ fragments used in eqn (2) are defined as follows:

2.4.1 R_{oNO3}. Organic nitrates, was given a value of 0.1, based on published measurements of organic nitrates.[49]

2.4.2 R_{calib}. For inorganic nitrate, is calculated as a static value from ammonium nitrate calibrations. The value varies in each AMS instrument and its history. As a result, the value of R_{calib} was slightly different between winter (0.79) and summer (0.70).

2.4.3 $R_{measured}$. The time-varying ratio of NO_2^+ to NO^+ ion fragments measured in the AMS during sampling.

Using these values, the fraction of organic nitrate signal of the total nitrate signal can be calculated as using the formula:[50]

$$oNO_{3,frac} = \frac{(1 + R_{oNO_3})(R_{measured} - R_{calib})}{(1 + R_{measured})(R_{oNO_3} - R_{calib})} \quad (2)$$

The fraction of inorganic NO_3 is therefore the difference between 1 and $oNO_{3,frac}$, and the mass of iNO_3 and oNO_3 is the fraction multiplied by the total nitrate signal. While the detection limits of individual fragments were verified throughout each season, no detection cutoff was used for separating organic from inorganic, as suggested in Kiendler-Scharr (2016).[50]

2.5 Positive matrix factorization

Positive matrix factorization (PMF) was used to analyze the organic aerosol (OA) in each season. PMF[51] is a receptor model that mathematically decomposes a total signal into a linear combination of factors. This technique can identify the relative contributions of OA types for AMS data.[52,53] Determination of the final PMF result for each season included comparisons between seasons and with published spectra, which will be discussed in the results section. For each season, PMF was applied to the organic mass spectral matrix using the data from both indoor and outdoor inlets collectively. Additionally, indoor only and outdoor only datasets were analyzed separately to confirm the consistency of the PMF solutions between the individual (indoor-only and outdoor-only) and the combined dataset. We present only the results of the combined dataset here.

2.6 Aerosol liquid water from Köhler theory

The aerosol liquid water content in each environment was calculated as a function of relative humidity and their chemical composition. Petters and Kreidenweis[54] proposed a single value to account for the hygroscopic properties of a chemical species using κ, defined by the relationship between the volume of the dry particle V_S, the volume of water V_W, and the water activity a_w as:

$$\kappa_i = \frac{V_W}{V_S}\left(\frac{1}{a_w} - 1\right) \quad (3)$$

assuming the Zdanovskii–Stokes–Robinson (ZSR) rule of mixing applies, a multi-component mixture κ_{mix} can be described as the sum of the κ of individual components, i, weighted by the volume fraction (ε) of that component:

$$\kappa_{mix} = \sum_i \varepsilon_i \kappa_i \quad (4)$$

For use with AMS data, the form of the measured species (*i.e.* SO_4 as H_2SO_4 or $(NH_4)_2SO_4$, *etc.*) was based on a pairing scheme for inorganics[55] and the fraction of signal at m/z 44 (f_{44}) for organics.[40]

The growth factor (GF) at any relative humidity is described by the ratio of the diameter of a wet particle at that relative humidity, D_{RH}, and dry diameter $D_{0,}$ or $GF = D_{RH}/D_0$. Rearranging and converting the diameters to spherical volumes and using eqn (3) and (4), the growth factor of a multicomponent mixture at a given RH (here a_w used as equivalent to fractional RH), is calculated by:

$$GF_{mix} = \left(\sum_i \varepsilon_i (GF_i)^3\right)^{1/3} \quad (5)$$

and the aerosol liquid water (ALW) of an aerosol at that RH can be calculated by:

$$\mathrm{ALW} = V_S(\mathrm{GF}_{mix}{}^3 - 1) \quad (6)$$

With a known aerosol composition *via* the AMS and aethalometer, the dry volume can be calculated. Of note, this calculation does not explicitly require a known aerosol diameter or size distribution, and does not take into account hysteresis effects which could be important in this dataset, since T and RH extremes in each season will occur in the HVAC system. We do not have measurements of T and RH in the HVAC, and calculations of aerosol liquid water therefore reflect the conditions of the indoor classroom or outdoors.

3. Results and discussion

3.1 Meteorological conditions

Fig. 1 shows the measured indoor and outdoor temperatures for the two measurement campaigns discussed here. Seasonal differences in Philadelphia are clearly observed in temperature differences and variability (*e.g.* $T_{average} \pm$ standard deviation). Outdoor T was 27 ± 3 °C during summer and 4 ± 6 °C during winter. Extremes in winter temperatures were coincident with storms with a low of −14 to a high of +18 °C. Summer temperatures fluctuated almost exclusively in diurnal patterns. RH varied over a similar range in each season, summer 62 ± 15% and winter 56 ± 17%, but again diurnally dependent in summer with winter RH driven by larger scale meteorological influences. The winter season experienced episodes of higher wind speeds (>6 m s^{-1}) corresponding to winter storms that brought snow while summer thunderstorms were not associated with high wind. Occasional summer thunderstorms brought changes in T and RH but not in measured aerosol species. Full meteorological data can be found in Fig. S2.†

Indoor T in both seasons varied very little: virtually unchanging (18 ± 1 °C) in summer, and in winter (22 ± 3 °C), somewhat influenced by a period of extreme cold (below −10 °C outdoors corresponding to the indoor minimum) with measurable warming while occupied. The RH, however, varied greatly during the winter (26 ± 9%), roughly following temperature fluctuations outdoors, and was constant in summer (55 ± 2%), regardless of outdoor RH. This constant indoor RH is expected from thermally well-controlled environments, including classrooms and offices. Comparisons of environmental conditions between indoors and outdoors as shown in Fig. 1 indicate that the HVAC system in both winter and summer was largely independent of weekday/weekend variations, and mostly independent of outdoor conditions with the exception of the very cold outdoor period in winter lowering indoor T by several degrees.

To understand the effects of both environments, the T and RH gradients between outdoors and indoors were used to investigate compositional changes between environments. The temperature gradient is defined as (indoor T − outdoor T), and the RH gradient defined as (outdoor RH − indoor RH). These were defined so that for both gradients, positive values indicate conditions that promote volatilization or thermodynamic aerosol losses, and the negative values are conditions that favor condensation or thermodynamic aerosol addition. This gradient difference was not prescribed as in thermodenuder experiments, but a result of natural outdoor variations and HVAC control of indoor conditions. The two-dimensional T and RH gradients for both winter and summer measurements are displayed in Fig. 2. The grid areas in Fig. 2 are colored by the number of measurements corresponding to that particular combination of T and RH gradients. Together, the two seasons span RH gradients from −18 to +62%, with significant overlap between seasons. The T gradients span from −18 to +29 °C and do not overlap between seasons. This set provides interesting analytical continuity in humidity, but with seasonal-based distinctions in temperature. An important note is the largest T gradient (∼+25 °C) corresponds to the lowest T conditions in both environments (∼−10 °C outdoors, ∼15 °C indoors). Additionally, we note that the indoor temperature in summer was ∼4 °C cooler than the average indoor temperature in winter.

3.2 PMF results

PMF results from both seasons identified three organic aerosol (OA) factors in common: oxygenated (OOA), hydrocarbon-like (HOA), and cooking (COA) aerosol. In summer, an additional factor contained significant contribution of reduced-nitrogen

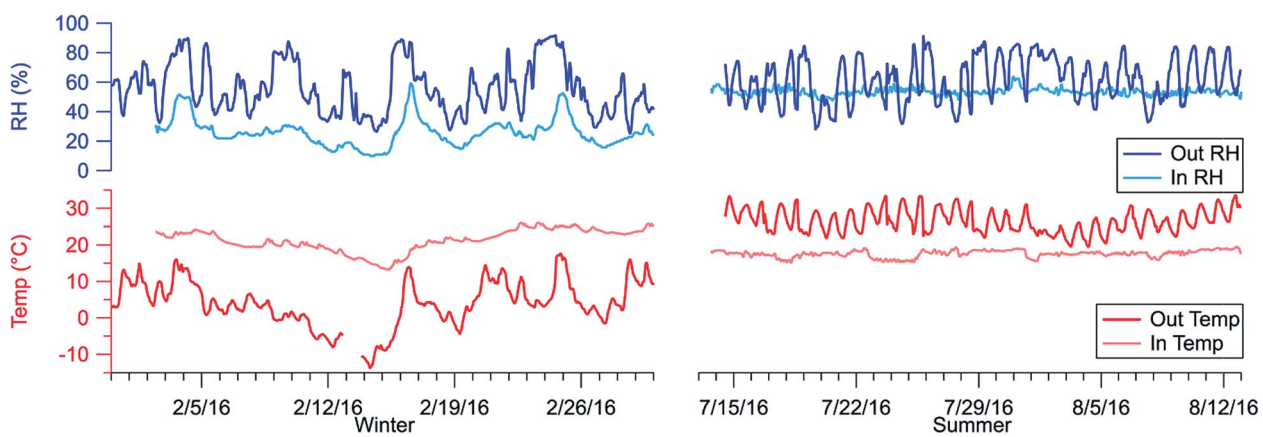

Fig. 1 Measured outdoor and indoor temperature (red lines) and relative humidity (blue lines) in winter and summer seasons.

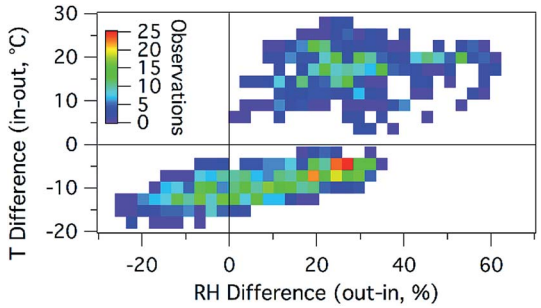

Fig. 2 Heat map showing the temperature and relative humidity differences between the indoor and outdoor environment. Pixel color shows the number of observations of a specific temperature and RH difference, white color indicates no observation. During winter, temperature and RH differences were all greater than 0, but during summer, the temperature gradient was negative and the humidity gradient varied. However, the number of points at each temperature and humidity gradient varied greatly, even sometimes for gradients near each other.

species linked to third hand smoke (THS). This factor was found to be predominantly indoors (median I/O = 7.6) and has been discussed separately.[15] Full mass spectra for each factor and each season are shown in the SI Fig. S3.† While the PMF results here are common between seasons, each season was investigated and the appropriate PMF solution was determined separately. Therefore, there are some seasonal differences between them. Diurnal variations discussed in the next section further support the factor identification for each season. Correlation with published spectra was generally higher for wintertime factors than summertime, so for convenience, the correlation values listed here are only the lower of the two seasons.

In both seasons, OOA was more similar to low volatility oxygenated OA (LV-OOA, $R^2 > 0.9$) than semi-volatile oxygenated OA (SV-OOA, $R^2 > 0.72$)[56,57] published factors. However, between less-oxidized oxygenated OA (LO-OOA) and more-oxidized oxygenated OA (MO-OOA), the OOA correlated slightly better with LO-OOA ($R^2 > 0.92$) than MO-OOA ($R^2 > 0.89$).[58] Between winter and summer, the two OOA factors correlated very well ($R^2 = 0.97$). However, wintertime OOA was less oxidized and exhibited a lower O/C ratio and higher H/C ratio (winter O/C 0.43 and H/C 1.31; summer O/C 0.59 and H/C 1.23).

HOA was characterized by prominent mass fragments at unsaturated and saturated hydrocarbon chain pairs m/z 41 and 43 (C_3H_5 and C_3H_7), and m/z 55 and 57 (C_4H_7 and C_4H_9), which are representative of lubricating oils and incomplete combustion and.[59,60] HOA was highly consistent between seasons ($R^2 = 0.93$) and well correlated with other urban HOA spectra ($R^2 > 0.90$).[56,58,61] The ratios of H/C 1.83 and 1.84, O/C 0.1 and 0.05 for summer and winter respectively further indicate the robustness of this factor mass spectrum across seasons.

COA was characterized by both oxidized and unoxidized fragments at m/z 43 (C_2H_3O and C_3H_7) and m/z 55 (C_3H_3O and C_4H_7), due to aliphatic acids from cooking oils and meat, and was somewhat different between seasons, due to significant contribution from more oxidized fragment components $C_2H_3O^+$ and CO_2^+ in summer. Wintertime COA (O/C 0.11, H/C 1.61) correlates very well with previously published wintertime spectra ($R^2 = 0.95$),[61] but inter-seasonal correlation is the lowest of the three at $R^2 = 0.79$. Identification of COA in the summertime was more dependent on the overall fragment signature of mixed hydrocarbon and oxidized series above m/z 50 and a diurnal pattern corresponding to the nearby food vendors. Summertime O/C 0.21 is high (and H/C 1.41 low) for COA, and may be a result of some spectral mixing with the OOA factor. In general, O/C ratios for all factors were higher in summer than winter.

3.3 Seasonal trends in outdoor aerosol composition

Total submicron outdoor aerosol concentrations were similar between seasons with an average of 6.96 μg m^{-3} in winter and 9.21 μg m^{-3} in summer, and ranged from 2.58 to 25.9 in the summer, and 0.63 to 24.7 μg m^{-3} in the winter. Compositional differences were notable between seasons. Outdoor organics, ammonium sulfate, and black carbon were slightly higher in summer, while ammonium and nitrate were much higher in winter. Average concentrations for all species can be found in Table 1. Summer was characterized by consistent and stable high organic aerosol, comprising 74% of AMS-measured species. In wintertime, that fraction was reduced to 52%, closer to other urban areas in humid continental climate zones.[11–13,62] Winter was characterized by storm meteorology-driven highs and lows, as well as short duration spikes in organic aerosol concentration, likely from local sources. Complete time series of the outdoor concentrations in this work are displayed in Fig. 3. Stagnation and high RH in winter produced prominent peaks in ammonium nitrate, with concentrations exceeding the organic aerosol concentration. High nitrate (20 to 30%) is common in wintertime traffic-dominated cities[61] due to its semi-volatile tendency to preferentially partition to the particle phase at ambient winter temperatures, but to the gas phase at summertime temperatures. In summer, overnight (10 PM to 2 AM) spikes in sulfate

Table 1 For each season and aerosol component, the campaign-average concentration, and quartile statistics for $(I/O)_{i/SO_4}$ as visualized in Fig. 6

Species or factor	Winter conc. (μg m^{-3})		Summer conc. (μg m^{-3})		Percentiles for $(I/O)_{i/SO_4}$ winter			Percentiles for $(I/O)_{i/SO_4}$ summer		
	Out	In	Out	In	25th	50th	75th	25th	50th	75th
SO_4	0.86	0.28	1.40	0.43	—	—	—	—	—	—
NH_4	0.63	0.07	0.44	0.05	—	—	—	—	—	—
NO_3	1.35	0.13	0.23	0.04	0.24	0.35	0.49	0.59	0.75	0.93
iNO_3	1.11	0.09	0.11	0.01	0.17	0.28	0.41	0.43	0.65	0.91
oNO_3	0.24	0.04	0.11	0.03	0.43	0.57	0.72	0.64	0.79	0.96
Org	3.24	1.14	5.98	2.22	0.88	1.00	1.17	1.07	1.17	1.29
HOA	0.69	0.29	0.46	0.26	0.94	1.24	1.77	1.36	1.96	2.89
COA	0.69	0.33	1.69	0.43	1.00	1.24	1.70	0.66	0.75	0.88
OOA	1.85	0.53	3.72	0.63	0.71	0.82	0.91	0.41	0.51	0.59
BC	0.62	0.25	0.74	0.41	0.93	1.18	1.62	1.29	1.80	2.80
THS	—	—	0.14	0.88	—	—	—	—	—	—
Total	**6.96**	**1.94**	**9.21**	**3.25**	—	—	—	—	—	—

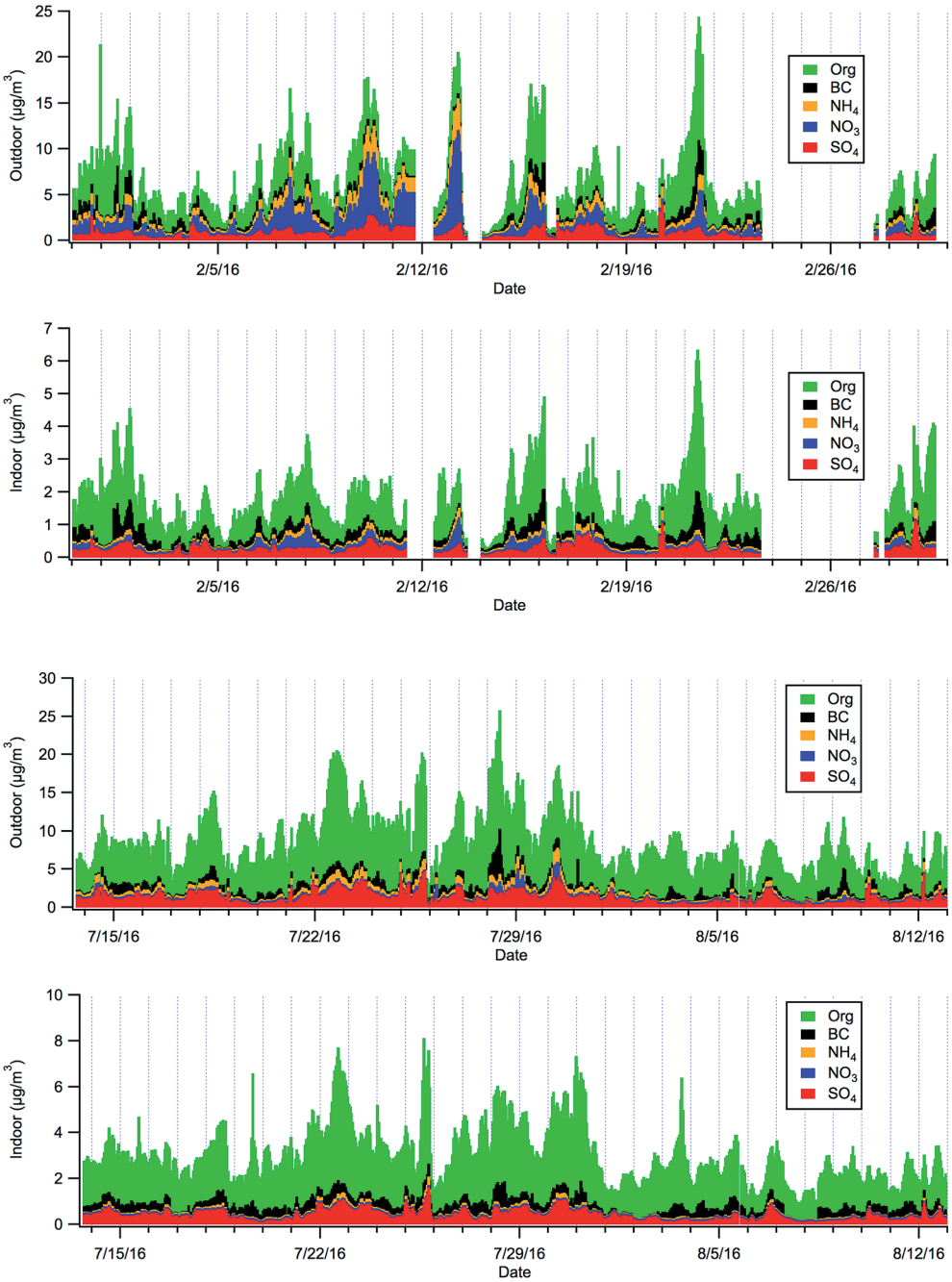

Fig. 3 Full stacked time series of AMS and aethalometer data for outdoor and indoor in winter (top pair) and summer (bottom pair).

and corresponding ammonium from an unidentified source were common.

3.3.1 Outdoor aerosol species trends and diurnal patterns. Summary average diurnal patterns of all measured aerosol species can be found in Fig. 4. Outdoor sulfate concentrations (panels a, b) showed little variation in diurnal pattern and similar concentrations across seasons near 1 μg m^{-3} indicative of regional (non-local) steady emissions. Ammonium is associated with both semi-volatile nitrate and non-volatile sulfate, and its diurnal pattern reflects that combined effect.

Aerosol nitrate shows very different seasonal trends. In the winter dataset, aerosol nitrate is predominately inorganic and is the largest inorganic contributor to aerosol mass. During episodic buildup of aerosol mass, some peaks exceeded 4 μg m^{-3} which were 3 × the study average (see Fig. 3). The diurnal pattern of nitrate in the winter (Fig. 4c) shows the highest concentrations at night, with the minimum during early afternoon hours. In winter, only 15% of total nitrate is organic nitrate. The organic nitrate diurnal pattern is different from inorganic nitrate, showing a slight increase in concentration around 7 AM, and peak concentration during the daytime hours. In the summertime dataset, total nitrate is a weak contributor to aerosol mass with a summertime average concentration at only 11% of the average winter concentration

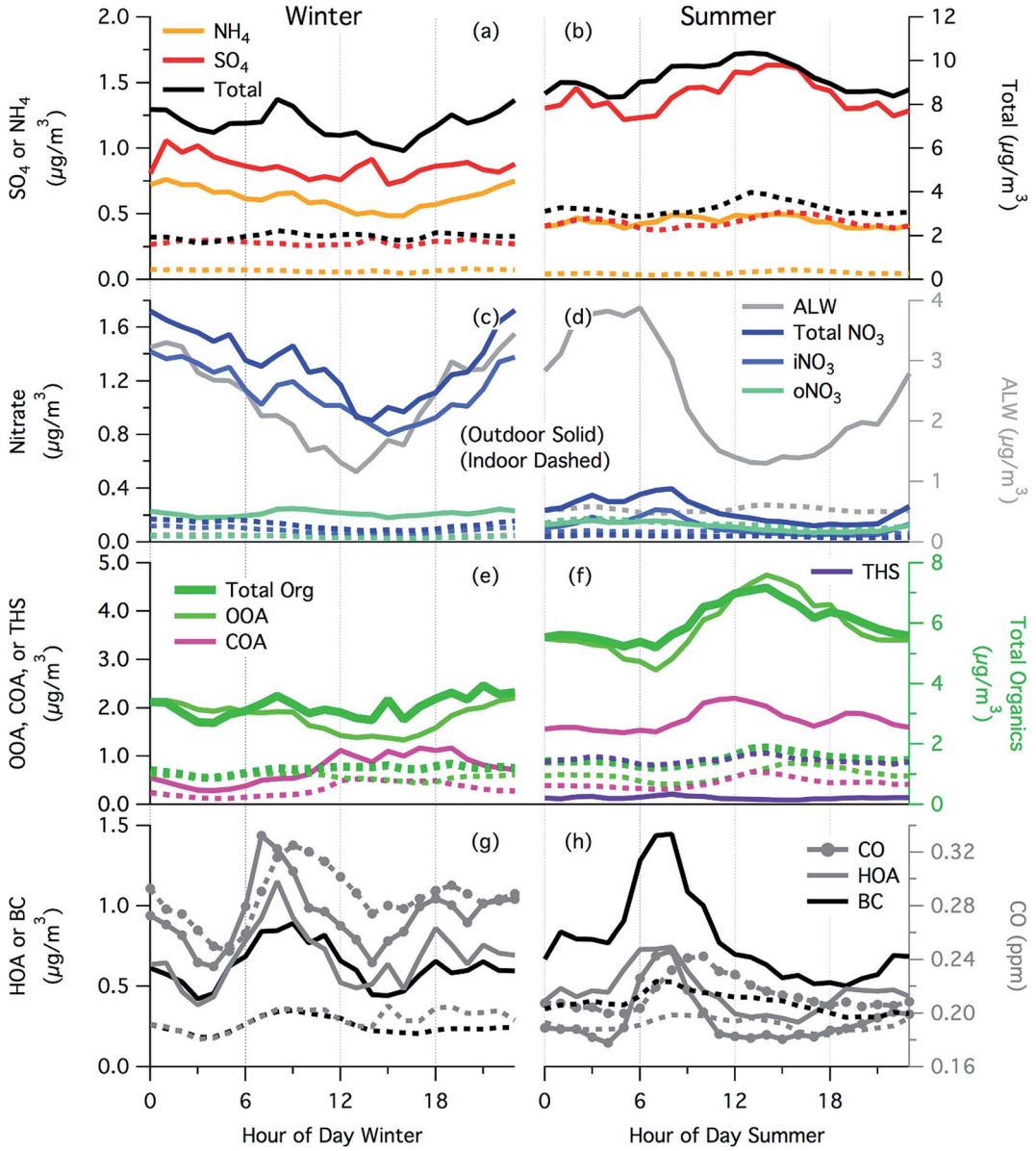

Fig. 4 Median diurnal patterns of each measured and calculated aerosol species in winter (left) and summer (right) as outdoor (solid) and indoor (dashed) lines. Sulfate, ammonium, and aerosol liquid water (a, b), total nitrate and its organic and inorganic fractions (c, d), total organics and the PMF components (e, f), and traffic-related components (g, h) of BC, CO, and HOA. Summertime nitrate (d) is magnified by 5 for visual enhancement, and the PMF factor THS was only observed in summer (f) and not winter (e).

of nitrate. Most of this seasonal difference comes from much lower inorganic nitrate concentrations, which in summer is only 7% of that in winter, while summer organic nitrate is a more comparable 37% of winter organic nitrate concentration. This observation is consistent with inorganic nitrate being more volatile as compared to organic nitrate, and consequently less likely to be in the aerosol phase. In summer, organic and inorganic contributions to total nitrate signal are roughly equal.

Aerosol liquid water (ALW) in winter has an average outdoor and indoor concentration (±standard deviation) of 2.6 ± 3.9 μg m^{-3} outdoors and only 0.11 ± 0.06 μg m^{-3} indoors. In summer, the decrease in concentrations upon transport indoors is much smaller, and similar to aerosol species at 2.7 ± 2.5 μg m^{-3} outdoors and 0.53 ± 0.24 indoors. This mass concentration is similar in concentration to all of the inorganic species combined. The ALW concentration follows the diurnal trends in RH and nitrate as described above, but is much more consistent across seasons. The implications of indoor ALW are discussed further in Section 3.4.

COA diurnal patterns (Fig. 4e and f) show different patterns by season. Both summer and winter show COA concentrations that start to increase around 9 AM and reach a maximum around lunch time. This trend is likely strongly influenced by the nearby food truck emissions as seen previously.[14] Food trucks end service around 6–7 PM, and in the winter dataset the decrease in COA diurnal concentration follows that trend. The

summertime diurnal pattern demonstrates a decrease in COA concentration after lunch followed by a second peak in COA concentration during evening hours (6 to 8 PM). This second peak in summertime COA may be indicative of influence from additional cooking sources in the larger area around the sampling site. Outdoor cooking and grilling is common throughout the city and much more common in the summertime than other seasons.

Seasonal differences in the OOA diurnal cycle (Fig. 4e and f) are clearly apparent. Summer OOA has a diurnal pattern which peaks during the early afternoon similar to ozone indicating photochemical production as has often been seen.[63,64] However, the wintertime OOA diurnal pattern decreases during the day, likely due to boundary layer dilution (see Fig. 5 for meteorological and gas-phase indicators of boundary layer). This decrease in concentration also follows trends in aerosol inorganic nitrate and RH, suggesting possible dependency on an aqueous phase, while the opposite is observed in summer.

Black carbon, CO, and HOA (panels g, h) exhibit diurnal patterns consistent with traffic emissions in each season, with CO and HOA having the most similar pattern. In contrast with CO and HOA, concentrations of BC were higher in summer than winter, resulting in a higher HOA/BC ratio during the colder winter measurements as compared to the summer. HOA/BC ratios have been discussed at length previously[65] and will be compared between indoors and outdoors below.

3.3.2 Indoor aerosol species trends and diurnal patterns. Indoor aerosol concentrations (dashed lines in Fig. 4) in both seasons are characterized by low nitrate, ammonium, COA, HOA, and ALW. All measured aerosol components follow the temporal trends of their outdoor counterparts, albeit at lower concentrations (the one exception is the third hand smoke

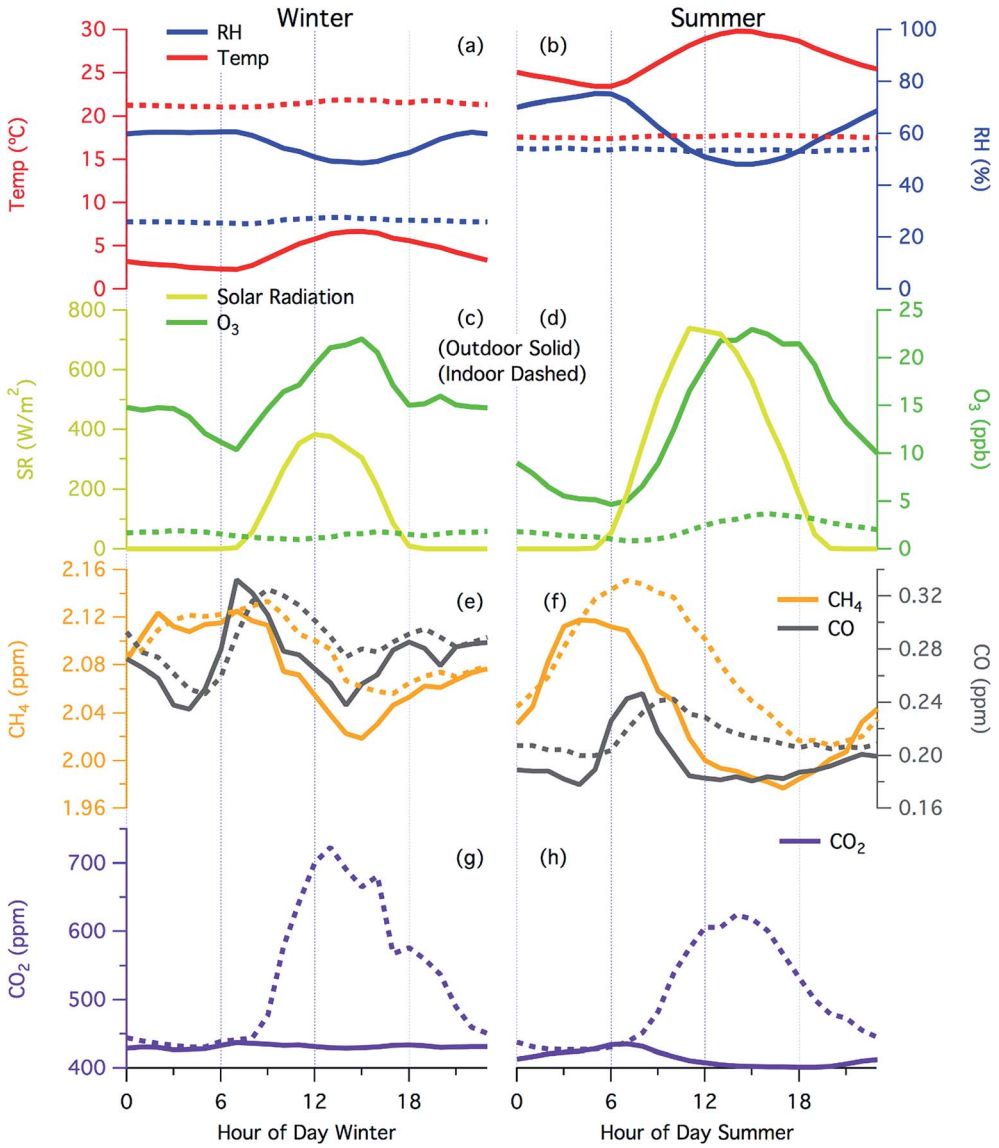

Fig. 5 Average diurnal patterns of meteorological data and measured gas-phase species in winter (left) and summer (right). Temperature and humidity (a, b), solar radiation and ozone (c, d), methane and CO (e, f), CO_2 (g, h). With the exception of CO_2 (indoor on left axis and outdoor on right axis), outdoor are shown in solid lines and indoor in dashed lines.

factor (THS) which described in depth elsewhere[15]). Nitrate is especially low, even when it is high outdoors in winter, and barely contributes indoors with average concentrations of organic and inorganic nitrate < 0.1 μg m^{-3} in both seasons. In addition to the lower concentrations observed indoors, each aerosol component shows a smoothed timeseries, and lags behind outdoor concentration fluctuations due to ventilation rate and mixing considerations. Importantly, some components like sulfate are similar across seasons. OOA in each season does vary with time of day, but less dramatically than outdoors. Black carbon consistently follows outdoor levels in both seasons as expected for a non-volatile, outdoor primary aerosol source.

Indoor HOA in summer did not track the outdoor HOA well during the daytime similar to previous observations.[14] HOA/BC values in both seasons show an increase indoors compared to out. In the winter measurements, the HOA/BC value increased from 1.12 (R^2 = 0.66) outdoors to 1.46 (R^2 = 0.53) indoors. Summertime HOA/BC values increased from 0.52 (R^2 = 0.33) outdoors to 1.54 (R^2 = 0.14) indoors, although the correlation at low loading was poor. Since BC is a non-volatile tracer and generally associated with diesel emissions in the absence of strong biomass signal, and HOA is a volatile species,[24,26] variations in the HOA/BC ratio are indicative of mass addition of chemical species similar to HOA. The outdoor HOA/BC ratio is inversely correlated with outdoor temperature in both seasons (R^2 = 0.24). These relationships are shown in more detail in Fig. S4.†

3.3.3 Outdoor gas-phase trends and diurnal patterns. Measured gas phases species showed seasonally-dependent trends. Meteorological and gas-phase diurnal average patterns are shown in Fig. 5. All measured gas-phase species (CO_2, CO, CH_4, O_3) demonstrated a similar pattern between seasons, but diurnal variations are less pronounced, and concentrations are generally higher in winter than summer. Measured CH_4 concentrations were slightly higher in the wintertime (panels e, f). Summertime CH_4 diurnal trends showed a more pronounced cycle, 0.05 ppm lower at the daytime minimum than in wintertime. CO was elevated during traffic rush hours along with enhanced concentrations of BC and HOA, as shown in Fig. 4. CO_2 followed the combined trends CH_4 and traffic-associated CO. While the diurnal pattern of ozone in the summer is more pronounced, the peak ozone values were similar between seasons. However, as Fig. 5 shows, ozone outdoors in summer rose and fell in specifically diurnal patterns, while ozone in winter was relatively constant and elevated (except for times of CO, CO_2, and CH_4 plumes). Concurrent plumes of CH_4, CO, and CO_2 exceeding 0.5 ppm CO and 2.6 ppm CH_4, coinciding with negligible ozone, lasting ~12 hours occurred in winter. A full time series of these species can be found in Fig. S5.†

3.3.4 Indoor gas-phase trends and diurnal patterns. Indoors, concentrations of CO and CH_4 indicate a little to no contribution from indoor sources, and are predominantly controlled by air exchange with the outdoors. The diurnal pattern of CH_4 (Fig. 5) indicates that the average CH_4 is higher indoors than outdoors, which is the result of low ventilation rate (0.4 h^{-1} in winter and 0.17 h^{-1} summer) and/or potentially influenced by a small unidentified indoor source. Peaks in outdoor CO and CH_4 linger indoors long after the outdoor concentrations return to background values, especially in summer when the ventilation rate was lower. This effect is observed in Fig. S5.† The CO_2 concentration indoors fluctuated during weekdays due to occupants in both in the classroom itself and the rooms on the same HVAC zone. In summer, when the room (but not the HVAC zone) was generally unoccupied (no scheduled classes), the peak CO_2 reached 872 ppm, compared with wintertime concentration peaking at 1110 ppm when scheduled classes were common. This seasonal difference is also observed in the daily patterns of CO_2 concentrations. Summertime CO_2 followed a smooth pattern of gradual rise in the morning and fall in the evening due to no direct emissions in the classroom and the well mixed recirculated air smoothing the impact of occupancy throughout the HVAC zone. However, in winter, the direct influence of classroom occupant emissions is visible with CO_2 concentrations showing steep increases and decreases multiple times in a single day, and the impact of evening classes as an additional bump in the winter CO_2 diurnal. Ozone concentration is nearly always close to detection limit of 1 ppb indoors, due to indoor deposition and reaction mechanisms that have been widely described previously.[66–68] That said, the summer indoor concentration does show increases with outdoor photochemically produced O_3 in mid-afternoon. Products of ozone reactions, especially with occupants, will be examined in future work.

3.4 SO_4 normalized I/O ratios

The sulfate-normalized indoor/outdoor ratio, denoted herein as $(I/O)_{i/SO_4}$ (see Section 1.2), of each species and PMF factor from AMS and aethalometer data is displayed in Fig. S6,† and summarized in Fig. 6 and Table 1. Nitrate and the OOA factor all have median $(I/O)_{i/SO_4}$ ratios less than unity, indicating an additional loss mechanism compared to sulfate in both seasons. In contrast, black carbon, HOA, and COA have median $(I/O)_{i/SO_4}$ ratios greater than unity, indicating either less loss than sulfate from filtration and deposition, or an additional indoor source. Inter-seasonal trends reveal more about the behavior of each species.

Observed trends in nitrate are consistent with its semi-volatile nature. The heating of buildings well over the outdoor temperatures in winter drives more nitrate components into the gas phase than in the summer when the outdoor-to-indoor temperature gradient is reversed. In both seasons, $(I/O)_{NO_3/SO_4}$ is less than unity, with median value of 0.35 in the winter and 0.75 in the summer, indicating no source indoors or condensation of nitrate components from the gas phase. Even with cooler indoor temperatures compared to outdoors in the summer, nitrate still shows losses in addition to those attributable to mechanical loss by filtration and deposition. The $(I/O)_{i/SO_4}$ of organic (oNO_3) and inorganic (iNO_3) nitrate in each season follows a similar trend with higher $(I/O)_{i/SO_4}$ ratios in the summer than winter (seasonal differences in NO_2^+ to NO^+ ratio are shown in Fig. S7†). Fig. 6 illustrates that overall oNO_3 have consistently higher $(I/O)_{i/SO_4}$ ratios than iNO_3 in both seasons.

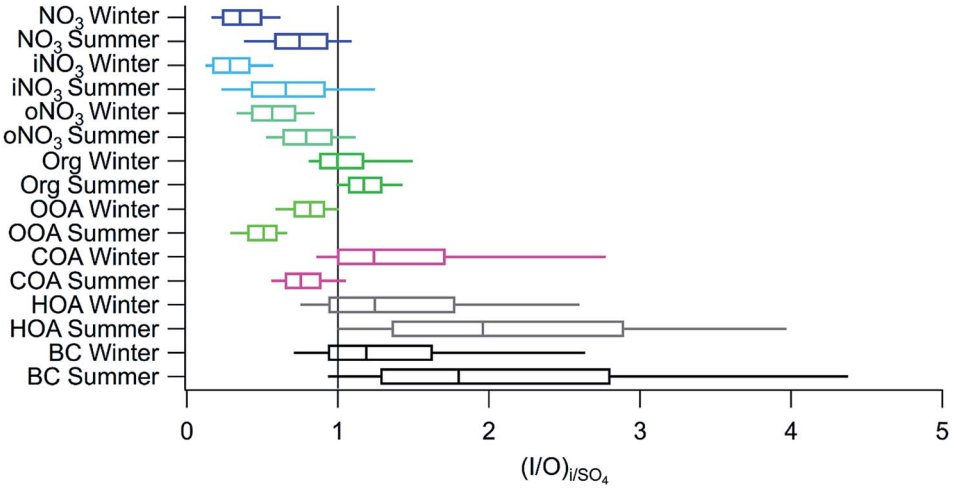

Fig. 6 The sulfate-normalized I/O ratio ($(I/O)_{i/SO_4}$) for each chemical component in each season. Values less than one indicate additional losses such as volatile losses, while greater than one indicates fewer losses or an indoor source.

This trend is likely reflective of volatility differences between oNO_3 and iNO_3. Note that the normalized I/O ratios for iNO_3 in summer span a very wide range due, in part, to its low concentrations and associated error when taking ratios of low concentrations.

Both HOA and BC show significantly higher concentrations outdoors than indoors, and their indoor concentrations are likely due to outdoor sources in this classroom environment. Black carbon and HOA trend together and have similar $(I/O)_{i/SO_4}$ distributions in each season (BC and HOA median 1.18 and 1.24, respectively, in winter, and 1.80 and 1.96, respectively, in summer). Their $(I/O)_{i/SO_4}$ ratios are typically above unity, and vary similarly with a large spread across a wide range of values, indicating similar sources. In contrast with sulfate, which has a flat diurnal pattern indicative of a regional source, HOA and BC are strongly linked to traffic emissions with strong local and diurnal character. Their $(I/O)_{i/SO_4}$ ratios are also typically above unity, potentially because black carbon and HOA may have less indoor mechanical losses than sulfate aerosol, and the $(I/O)_{i/SO_4}$ ratio implicitly assumes internal mixing and associated similar mechanical losses indoors.

It is likely that external mixing of aerosol populations may be the reason for this trend, since on short timescales when mixing freshly emitted traffic emissions into the regional plume there will be external mixing of aerosol populations (*e.g.* Rissler *et al.*[69]). Since the $(I/O)_{i/SO_4}$ ratio implicitly assumes internal mixing and similar mechanical loss, and this is not valid for external mixtures, values in both seasons above unity may be due to less mechanical (*e.g.* filtration and depositional) losses of these traffic particles.

Additionally, since summertime $(I/O)_{i/SO_4}$ values of BC and HOA are higher than values in wintertime, variations in the HVAC operation may explain that difference. Summertime RH levels and HVAC cooling coil operation will serve to increase water content of hygroscopic accumulation mode particles, potentially activating them to droplets, compared to the non-hygroscopic traffic related particles.[72] This could increase the effective size of accumulation mode particles in the summertime, and subsequent higher filtration efficiency may explain the higher $(I/O)_{i/SO_4}$ values for BC and HOA in that season. Fig. S8† shows that the size dependent filtration efficiency of m/z 57 (a proxy for traffic particles) has a more similar indoor/outdoor ratio than sulfate at smaller sizes and a higher ratio than sulfate at larger sizes.[70,71] This is more dramatic for the summer data than for winter, consistent with HVAC-associated losses of hygroscopic components. However, the I/O ratios of hygroscopic sulfate are comparable (0.35 in winter and 0.31 in summer).

A shift in the proportional contribution of different sources or age of BC between seasons could also contribute to this seasonal trend. Given the differences in slope and regression of the HOA/BC ratio between seasons (see Fig. S4†), there are likely some differences in emission sources between seasons. Additionally, wintertime build-ups of aerosol mass could have aged BC and made it more internally mixed with regional aerosol.

It is also important to note here that, previous work by Johnson *et al.* (2017)[14] found an enhancement of HOA indoors without a corresponding increase of BC. Using the same procedure to calculate BC-associated HOA indoors using the observed outdoor ratio shows that for this study most of the HOA indoors can be linked to BC and therefore due to outdoor-to-indoor transport (see Fig. S4†). While measurements for the previous study were done in the same building, they were performed in a separate part of the building with a different HVAC system and 100% outdoor air operation (no recirculation). Differences between these studies highlight the heterogeneity of indoor spaces even within the same building.

For OOA, the $(I/O)_{OOA/SO_4}$ value has a different seasonal relationship, with summer showing lower sulfate normalized ratios than winter. Seasonal differences in the OOA diurnal patterns indicate that much of the summertime OOA is formed locally through photochemical production due to its similar diurnal patterns as outdoor ozone, whereas the wintertime OOA appears to be more regional and therefore aged, and varies

inversely with boundary layer height. With this trend in mind, it is likely that the summer time OOA is more volatile than the wintertime OOA.[26,63] Additional losses may also be due to HVAC operational differences by season. Summertime air conditioning condenses water and gas-phase water-soluble materials in the aqueous films of the system cooling coil. We hypothesize that this process would lead to losses of water-soluble components as that water is drained and removed from the system and then replenished. Many types of OOA and their gas-phase counterparts are water-soluble. Depletion of gas-phase species through loss to aqueous films will lead to the need to re-establish equilibrium when the air leaves the HVAC system, resulting in loss of particle based OOA components to the gas phase, and likely contribute to the observation that $(I/O)_{OOA/SO_4}$ are less than unity in both seasons.[73]

COA exhibits the largest inter-seasonal variation in $(I/O)_{i/SO_4}$ in both median value and range. This variability is likely due to an indoor source of COA or an indoor source chemically similar to COA. Unlike other species where $(I/O)_{i/SO_4}$ is large (including HOA), inspection of the COA time series reveals several instances of indoor concentrations exceeding outdoor concentrations, with the (I/O) and $(I/O)_{i/SO_4}$ both greater than unity in the wintertime. Potential explanations for this include a cooking source from recirculated office air (the smell of toast was observed indoors) or differences in occupancy with regular classes in the winter, but not in the summer. This seasonal difference is important to note while discussing the seasonal gradients.

3.5 Dependence of $(I/O)_{i/SO_4}$ ratios on *T* and RH gradients

By combining winter and summer datasets, the trends in $(I/O)_{i/SO_4}$ ratios as a function of temperature and relative humidity can be investigated and extend the single season analysis by Johnson *et al.*[14] Data from each season was combined and *T* and RH bins were created by placing an equal number of points in each bin instead of an evenly-spaced temperature or humidity difference. This unfortunately creates non-uniform bin spacing (more pronounced in *T* data), but does not suffer from over-weighing sparse data. For example, there are very few measurements made for a *T* gradient between −5 and +5 °C but there are dozens of measurements made for a temperature gradient of −10 to −5 °C bin (see Fig. 2). Since the *T* differences are, by nature, segregated by season (winter positive, summer negative), and the RH differences are not (winter positive, summer both positive and negative), and the RH range is much larger, examining the ratios as a function of both *T* and RH provides important information.

The $(I/O)_{i/SO_4}$ values as a function of *T* and RH gradients between indoors and outdoors are shown in Fig. 7 and 8. Each plot shows the statistical distribution of $(I/O)_{i/SO_4}$ data as a box-whisker placed at the center of each *T* or RH bin. Regression analysis on median values for each $(I/O)_{i/SO_4}$ are provided for linear (black lines) and exponential (grey lines) fits to the full datasets, while linear regression for each season separately is demonstrated in red lines. The fit parameters for each analysis are provided in Table 2. Additionally, a non-parametric LOESS fit as a function of *T* and RH are provided in Table S2† which provides a stepwise linear fit to the data with no assumption of functional form. We provide the various regression analysis and fit parameters so that researchers who model the indoor environment may be able to choose a scheme to implement in indoor models of aerosol chemical species. Of note is that all linear regressions agree in sign with those discussed in Johnson *et al.*,[14] for a similar single-season analysis in a different location, except for those reported with effectively no correlation (R^2 < 0.1). As seen in Fig. 7 and 8, the overall directional trend of each species and PMF factor $(I/O)_{i/SO_4}$ are the same for both *T* and RH gradients. This is expected since *T* and RH gradients are broadly interrelated, with increases in *T* gradients having corresponding decreases in RH gradients. When split by seasons, summer linear fits are better for the summer data than for winter (except for BC). In general, the regressions are low due to invariance in the $(I/O)_{i/SO_4}$ ratio over the season rather than scatter (*i.e.* slopes < 0.01 correspond to R^2 < 0.6).

The behavior of total aerosol nitrate is shown in Fig. 7a. Total nitrate is lost in both seasons (almost all I/O ratio data is less than unity), with the exponential fit better capturing the flattening out at $(I/O)_{NO3/SO_4}$ of 0.37 for positive (in > out) *T* gradients. This flattening indicates that potentially some limiting factor could keep all of the nitrate from being completely removed. This effectively full removal at low positive *T* gradients could be why the regression for winter only is poor. This trend is also consistent with thermodenuder data showing nitrate remaining in the aerosol phase at temperatures exceeding 100 °C, albeit at higher values.[26] Inorganic nitrate (Fig. 7b) and organic nitrate (part c) have similar responses to the *T* gradient. However, the asymptote at high indoor *vs.* outdoor *T* of oNO_3 is higher than iNO_3, at 0.60 *versus* 0.31, respectively (see Table 2), which is consistent for a less volatile species. For RH gradients, a linear regression matches the trend for total nitrate, oNO3, and iNO3 very well (total nitrate R^2 = 0.95). Note that the *y*-intercepts 0.61, 0.52, and 0.72 for total, iNO_3, and oNO_3 respectively, are each less than unity. If *T* or RH gradients were the only loss mechanism beyond the mechanical losses observed for sulfate, the *y*-intercept from the linear regression for aerosol nitrate species should be unity. This lower *y*-intercept indicates that there is an additional loss process occurring in addition to mechanical, and *T* or RH gradient related losses.

Trends in $(I/O)_{Org/SO_4}$ *versus* *T* and RH are shown in 7d and are mostly all slightly above unity, with a weak decrease in *T* and RH gradients. The variation in $(I/O)_{Org/SO_4}$ values is small compared to nitrate with the box-whisker plots showing tighter distributions in the summer (negative *T* gradients). The separation of organics into components *via* PMF and the subsequent *T* and RH gradient analysis is shown in Fig. 8. This figure shows considerable differences in the various organic component behaviors. These changes largely offset each other, and explain why the observed total organic ratio $(I/O)_{Org/SO_4}$ is largely invariable.

Trends over the whole range of *T* and RH gradients for OOA are shown in Fig. 8, and indicate additional losses ($(I/O)_{i/SO_4}$ less than unity) for both *T* and RH gradients. The variations,

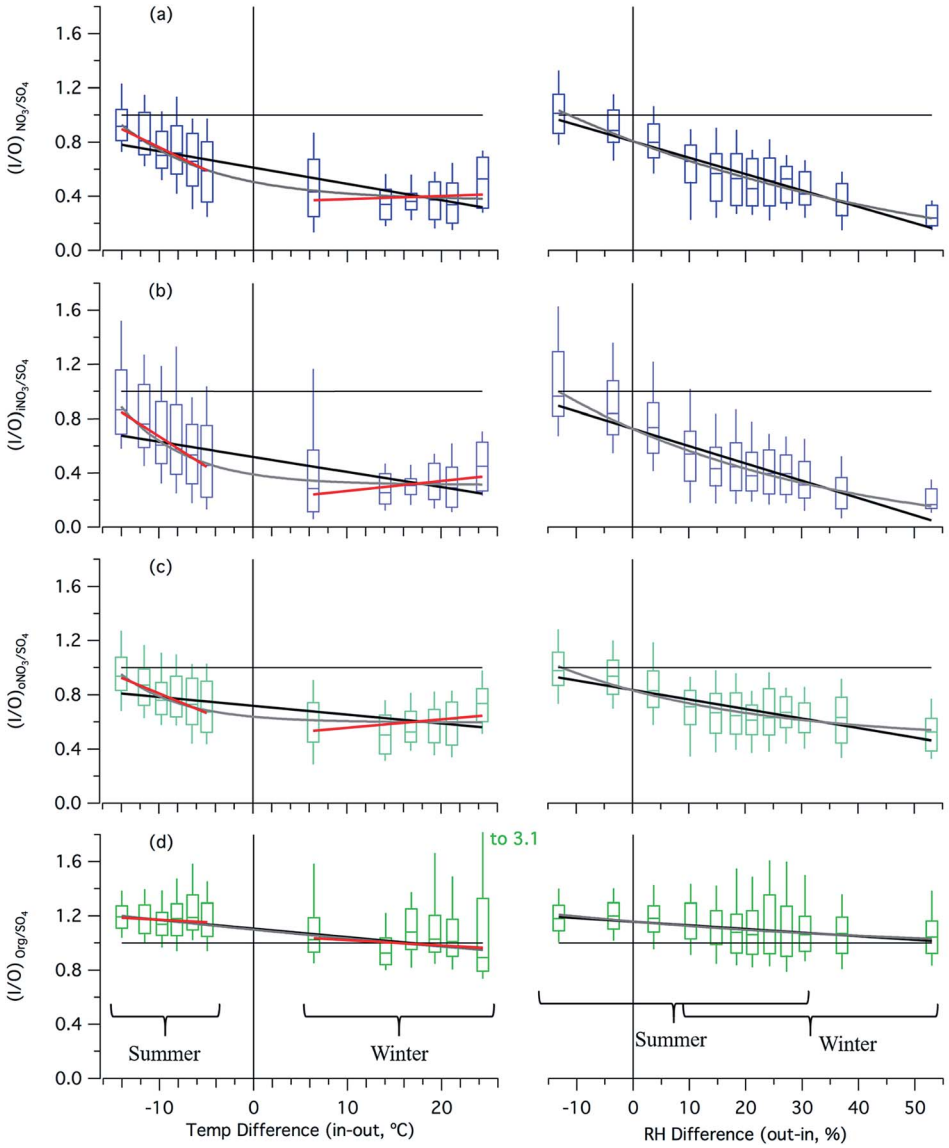

Fig. 7 Dependence of $(I/O)_{i/SO_4}$ on differences in temperature and humidity between environments for (a) nitrate, (b) inorganic nitrate (c) organic nitrate, and (d) organics data have been binned by temperature or humidity differences, and the regression is of the median value of each bin. Both temperature and humidity gradients favor volatilization in the positive direction. Complete statistics of the regression are listed in Table 2.

however, are not fit well and may be due to chemical differences in the OOA factor between seasons as discussed during the diurnal analysis. The *T* gradient plot (again, naturally separated by season) shows somewhat different trends between seasons, with a negative slope in summer (negative gradient values) and flat in winter. The positive trend between seasons is likely explained by the differences in OOA volatility and formation differences between the seasons as previously discussed in section 3.4. This potential difference in OOA between seasons complicates the RH gradient analysis where seasons overlap; this is observed in the broad distribution of ratios seen for the overlapping seasonal data in the 10 to 30% RH difference range. Fig. S9† shows the season-separated binning and regression lines, indicating that the summer regression has a negative slope while the winter is flat, similar to that observed with temperature gradients.

For COA, the *T* and RH gradients in $(I/O)_{COA/SO_4}$ more clearly shows disparities between seasons. In summer (negative *T* gradients) there appears to be a slight decrease in median $(I/O)_{COA/SO_4}$ similar to volatility-based removal, and all median values are less than unity. However, in winter (positive *T* gradients) the trend is reversed and the box and whiskers cover a much broader range. This again indicates a COA source indoors in winter that is not related to *T* or RH gradient. This is likely due to high occupancy in the winter with occupants and associated activities in adjacent spaces (*e.g.* use of toasters and other office cooking products). The human contribution to the indoor aerosol composition during the wintertime measurements will be discussed in a future publication. In summer,

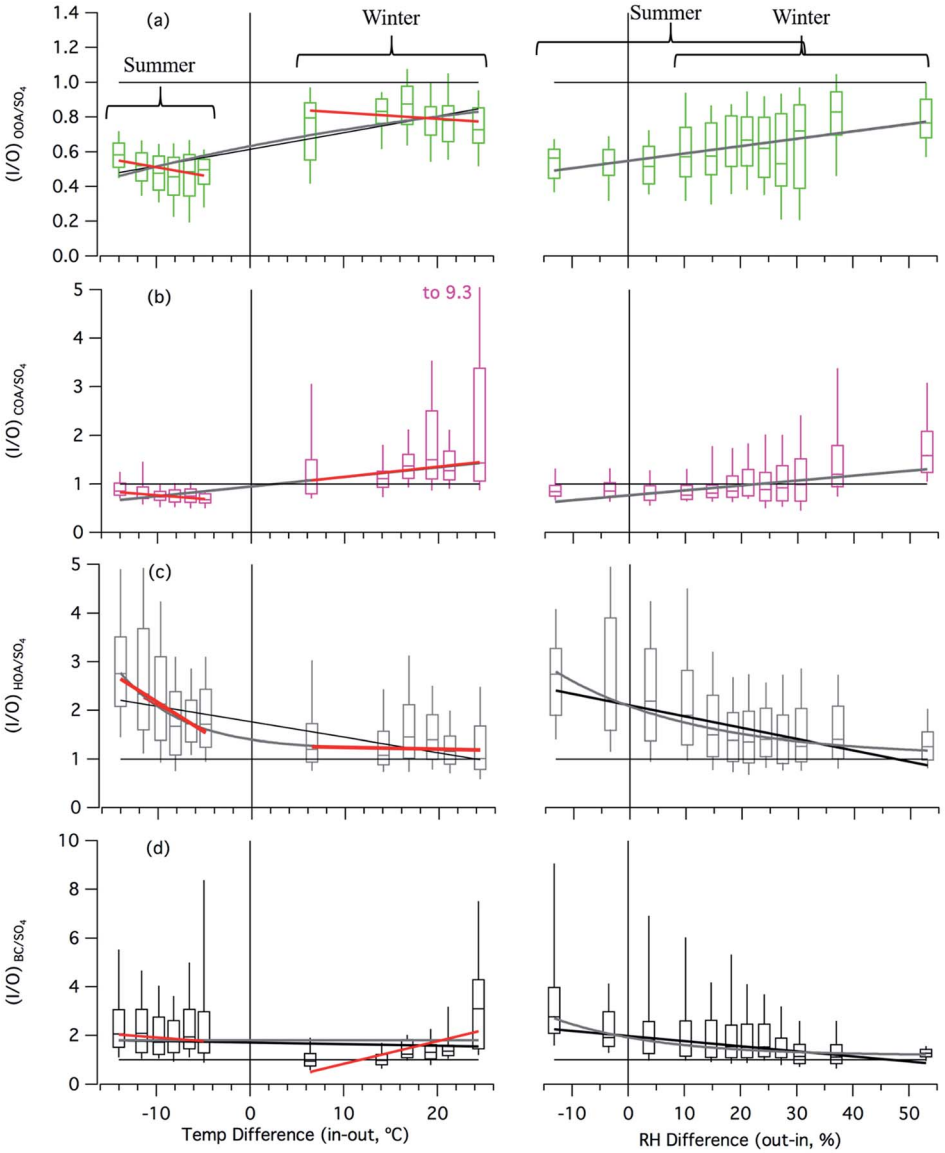

Fig. 8 Dependence of $(I/O)_{i/SO_4}$ on differences in temperature and humidity between environments for (a) OOA, (b) COA, (c) HOA, and (d) black carbon (BC). Data have been binned by temperature or humidity differences, and the regression is of the median value of each bin. Both temperature and humidity gradients favor volatilization in the positive direction. Complete statistics of the regression are listed in Table 2.

there were no scheduled classes and overall student activities were reduced. $(I/O)_{COA/SO_4}$ trends with RH gradient show an increase in value with increasing RH gradient, but this is complicated by seasonal overlap. For RH gradients observed in both seasons (bins encompassing +10 to 30% gradient), the $(I/O)_{COA/SO_4}$ values in the box whisker plot show broader distributions.

For HOA, the $(I/O)_{HOA/SO_4}$ trends are quite large in the summer (negative T gradient) and low RH gradient (<15%). Similar to the general seasonal analysis $(I/O)_{HOA/SO_4}$ is nearly always greater than unity with a clear trend in T and RH gradients. As discussed above, the $(I/O)_{HOA/SO_4}$ value greater than unity is likely due to external mixing of HOA containing traffic particles and sulfate containing accumulation mode particles. The strong dependence on T may be one or a combination of the following: additional gas to particle partitioning of HOA vapors at lower indoor T, enhanced loss of accumulation mode particles in relation to traffic related particles as a function of T, or an indoor source of HOA that is T dependent. Comparing the characteristics of HOA and BC as described below help to elucidate what mechanisms are dominant. From the results of the work discussed here, it is clear that there is evidence of external mixing and size dependent differences in I/O ratios for the AMS traffic related signal at m/z 57 (see Fig. S8†). Further work will need to be performed with additional sampling locations to address whether loss rate or potential sources (and location of those sources *e.g.* HVAC, room, *etc.*) of HOA are more important.

While the total $(I/O)_{HOA/SO_4}$ and $(I/O)_{BC/SO_4}$ statistics for each season are similar between HOA and BC (see Fig. 6), the trends

Table 2 For each AMS species or PMF-derived organic component, summary statistics of regressions for I/O ratios of components i normalized by the I/O ratio of sulfate $(I/O)_{i/SO_4}$ against indoor-to-outdoor temperature differences (ΔT_{in-out}) and humidity differences (ΔRH_{out-in})

Species or factor	Linear fit of $(I/O)_{i/SO_4}$ against multi-season ΔT_{in-out}			Exponential fit of $(I/O)_{i/SO_4}$ against multi-season ΔT_{in-out}		
	Slope	y-int	R^2	$y0$	A	τ
NO_3	−0.012	0.61	0.77	0.37	0.56	9.9
iNO_3	−0.011	0.52	0.66	0.31	0.58	7.04
oNO_3	−0.007	0.72	0.53	0.6	0.36	6.58
Org	−0.007	1.10	0.82	0.29	0.91	119.1
OOA	0.010	0.61	0.74	1.11	−0.65	45.1
COA	0.020	0.95	0.87	346	−345	1.7×10^4
HOA	−0.032	1.76	0.73	1.2	1.58	6.8
BC	−0.007	1.72	0.03	7.32	−5.51	1.87×10^{10}

Species or factor	Linear fit of $(I/O)_{i/SO_4}$ against multi-season ΔRH_{out-in}			Exponential fit of $(I/O)_{i/SO_4}$ against multi-season ΔRH_{out-in}		
	Slope	y-int	R^2	$y0$	A	τ
NO_3	−0.012	0.81	0.95	−0.23	1.27	66.6
iNO_3	−0.013	0.73	0.92	−0.013	0.73	0.92
oNO_3	−0.007	0.84	0.84	−0.007	0.84	0.84
Org	−0.003	1.16	0.81	0.93	0.29	67.2
OOA	0.004	0.55	0.58	67.8	−67.31	1.59×10^4
COA	0.010	0.77	0.64	467	−466	4.62×10^4
HOA	−0.023	2.10	0.77	1.06	1.74	24.8
BC	−0.021	1.98	0.74	1.17	1.54	18.2

Species or factor	Linear fit of $(I/O)_{i/SO_4}$ against summer ΔT_{in-out}			Linear fit of $(I/O)_{i/SO_4}$ against winter ΔT_{in-out}		
	Slope	y-int	R^2	Slope	y-int	R^2
NO_3	−0.034	0.42	0.95	0.002	0.36	0.04
iNO_3	−0.044	0.23	0.97	0.007	0.20	0.44
oNO_3	−0.029	0.53	0.94	0.006	0.49	0.22
Org	−0.004	1.14	0.22	−0.004	1.06	0.12
OOA	−0.010	0.41	0.52	−0.004	0.86	0.20
COA	−0.016	0.61	0.82	0.021	0.94	0.60
HOA	−0.122	0.93	0.88	−0.004	1.28	0.02
BC	−0.030	1.62	0.40	0.093	−0.10	0.52

versus T and RH gradients reveal differences. While $(I/O)_{HOA/SO_4}$ shows a decrease across T gradients from about 2.5 to just above unity, BC shows little variation across T gradients with $(I/O)_{BC/SO_4}$ ratios near 2 throughout. The consistently high $(I/O)_{i/SO_4}$ values (much greater than unity) for both HOA and BC are likely explained by relative loss rates of traffic and accumulation mode particles, but there is little change over T or RH gradients for non-volatile BC as compared to the volatile HOA. Since $(I/O)_{HOA/SO_4}$ has a stronger dependence on T than $(I/O)_{BC/SO_4}$ for the summer season, the most likely explanation for the observed HOA dependence is T driven partitioning. RH gradients for $(I/O)_{BC/SO_4}$ indicate some dependence of BC similar to that observed for HOA but not to the same magnitude.

HOA is known to be a semi-volatile OA component[24,26] while BC is not. As described in Section 3.3.1, the HOA/BC ratio changes between environments and between seasons: winter is higher than summer, and indoor is higher than outdoor in both seasons. However, the correlation in summer is poor compared with winter ($R^2 = 0.33$ *versus* $R^2 = 0.66$ outdoors), such that the relative contribution of different sources of HOA and BC are different. The outdoor HOA/BC ratio is correlated to outdoor T (slope = −0.009, $R^2 = 0.69$), across the almost 40 °C range of observed outdoor T, indicating volatility-based differences between BC and HOA contribute to differences between seasons and environments. However, the range of values in summer is considerably higher than winter (see Fig. S4†). Similarly, the I/O ratio of HOA/BC (of note, not normalized by sulfate), shows a weak decrease with T gradient (slope = −0.007, $R^2 = 0.24$), with what appears to be a downward slope in each season independently. There is no correlation with the I/O ratio per RH difference (slope = 0.0001, $R^2 < 0.01$).

3.6 Aerosol liquid water and implications for the indoor environment

Aerosol liquid water (ALW) calculated from Köhler theory has important implications for indoor chemistry and dynamics.[30] Outdoors, over the lifetime of aerosols, ALW influences partitioning and chemical transformation of both organic and inorganic aerosol components. The impact of ALW on organics outdoors is not completely understood, but it has been shown to participate in both reversible and irreversible uptake of organics.[74,75] In this work, the most water-soluble organic fraction, OOA, trends diurnally with ALW in winter, but the reverse is true in the summer, when outdoor OOA concentrations are strongly driven by photochemistry.

Indoors, an aqueous phase or surface is also an important part of understanding chemical behavior including partitioning, transformation, and subsequent exposure. Multiple studies have examined the importance of humidity on ozone-terpene reactions indoors, increasing mass loading and particle formation.[76–78] For this study, ALW indoors here is seasonally-dependent, with both seasons showing lower ALW indoors compared to outdoors.

ALW is driven strongly by the mass fraction of aerosol that is hygroscopic,[54] typically the inorganic salt components. In the wintertime, the average nitrate concentration was higher than summer, and additional build-up events lead to extremely high nitrate concentrations, and enhanced ALW outdoors. Upon transport to the indoor environment, the combination of heating and lower RH drives the nitrate out of the aerosol phase, and significantly reduces the ALW of indoor aerosol in the wintertime. In wintertime, the ALW difference between indoor and outdoor is dramatic with high (2.6 ± 3.9 μg m^{-3}) outdoors and extremely low (0.11 ± 0.06 μg m^{-3}) indoors. In summer, the lower-nitrate but humid environment outdoors gives similar but more consistent ALW 2.7 ± 2.5 μg m^{-3}. In contrast, summer indoor ALW is much higher than during winter indoors at 0.53 $\pm$ 0.24 μg m^{-3}. As ALW is calculated from dry mass concentrations, the mechanical removal of mass upon transport to the indoor environment contributes to the lower ALW

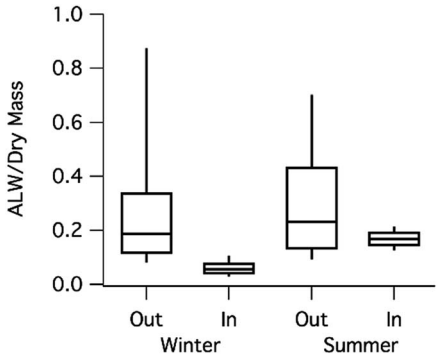

Fig. 9 Distribution of liquid water normalized by the measured dry aerosol mass for each season and environment. Winter and summer have similar distributions outdoors (although slightly larger distribution in winter), but in winter indoors, minimal ALW is observed, compared with summer.

concentration indoors. Therefore, the following section will discuss ALW as normalized to dry mass.

Fig. 9 shows the distribution of ALW per dry aerosol mass in each season and environment. Distributions of ALW are highly variable outdoors since neither T or RH are controlled. Maximum wintertime ALW are larger than in summer, but wintertime increases in hygroscopic nitrate are mitigated by higher humidity in summer, with the result of very similar ALW outdoors between seasons. In the indoor environment, ALW occupies a much smaller range of values due to the less variable T and RH conditions of the classroom. In winter there is no overlap between the indoor and outdoor environment, whereas the summer time shows the indoor ALW varying roughly between the 25^{th} and 50^{th} percentiles of the outdoor values.

Of importance to this discussion is also the role the HVAC system plays in both regulating the indoor classroom environment and providing an extreme of T and RH which changes seasonally. Wintertime aerosol passing through the HVAC system as part of the air intake or recirculation will be heated to temperatures of about 40 °C. These are the highest temperatures and lowest RH values the indoor air will experience, and will effectively dry out or effloresce aerosols. In summer, the HVAC system works to cool the air and exposes air in the system to temperatures of approximately 10 °C and generally increasing RH to 100%, driving deliquescence of aerosol particles and condensation of water on chiller coils. The ALW presented in Fig. 9 show the calculated values for the room conditions where the particles spend the vast majority of their time, but these values will be much higher for indoor aerosols in summer in the chilling portion of the HVAC and lower in winter in the heating section. Differences in aerosol composition and chemistry at various stages of transport to the indoor environment are beyond the scope of this study, but should be investigated in future work.

4. Conclusions

This investigation of seasonal trends of outdoor and indoor aerosols has improved our understanding of the link between indoor and outdoor air quality. The outdoor seasonal analysis shows trends similar to those expected of an urban area, as organics dominated outdoor aerosol in both seasons, and nitrate was a major component in winter but not summer. However, most human exposure to pollutants occurs indoors, and outdoor aerosols are transformed before reaching indoor spaces, and resulting indoor concentrations are a result of the contribution of individual aerosol components, the HVAC system influence, and the environmental conditions (*e.g.* T, RH). The sulfate normalized I/O ratio, called $(I/O)_{i/SO_4}$, was used to isolate chemically-specific changes to other aerosol species, beyond aerosol mechanical losses. The broad range of conditions sampled here, across several weeks in summer and winter seasons in a highly controlled indoor space, provides a comprehensive parameterization for analysis of these effects. The $(I/O)_{i/SO_4}$ of nitrate, total organics, HOA, and BC are higher in the summer season than winter, and the $(I/O)_{i/SO_4}$ are described as a function of outdoor and indoor T and RH gradients. These trends can be applied to indoor models to better inform indoor aerosol dynamics and exposure. Aerosol liquid water (ALW) influences aerosol processing and is generally available outdoors in both seasons, but ALW is nearly nonexistent in winter indoors, and higher but rather invariable in summer indoors. This trend in ALW can have important consequences for indoor chemistry. Connecting outdoor pollutants to exposure indoors is a key challenge for human health, and this work provides direct measurements of indoor and outdoor aerosols, and parameterizations directly applicable to future analyses.

Conflicts of interest

The authors have no conflicts of interest to declare.

Acknowledgements

Funding for this work was provided by the US National Science Foundation Award #: CBET-1437916.

References

1 F. Dominici, R. D. Peng, M. L. Bell, L. Pham, A. Mcdermott, S. L. Zeger and J. M. Samet, Fine Particulate Air Pollution and Hospital Admission for Cardiovascular and Respiratory Diseases, *J. Am. Med. Assoc.*, 2006, **295**, 1127–1134.
2 N. E. Klepeis, W. C. Nelson, W. R. Ott, J. P. Robinson, A. M. Tsang, P. Switzer, J. V. Behar, S. C. Hern and W. H. Engelmann, The National Human Activity Pattern Survey (NHAPS): A resource for assessing exposure to environmental pollutants, *J. Exposure Anal. Environ. Epidemiol.*, 2001, **11**, 231–252.
3 W. C. Malm, J. F. Sisler, D. Huffman, R. A. Eldred and T. A. Cahill, Spatial and seasonal trends in particle concentration and optical extinction in the United States, *J. Geophys. Res.*, 1994, **99**, 1347.
4 N. L. Ng, S. C. Herndon, A. Trimborn, M. R. Canagaratna, P. L. Croteau, T. B. Onasch, D. Sueper, D. R. Worsnop,

Q. Zhang, Y. L. Sun and J. T. Jayne, An Aerosol Chemical Speciation Monitor (ACSM) for routine monitoring of the composition and mass concentrations of ambient aerosol, *Aerosol Sci. Technol.*, 2011, **45**, 780–794.

5 Y. L. Sun, Z. F. Wang, W. Du, Q. Zhang, Q. Q. Wang, P. Q. Fu, X. L. Pan, J. Li, J. Jayne and D. R. Worsnop, Long-term real-time measurements of aerosol particle composition in Beijing, China: Seasonal variations, meteorological effects, and source analysis, *Atmos. Chem. Phys.*, 2015, **15**, 10149–10165.

6 S. Takahama, A. Johnson, J. Guzman Morales, L. M. Russell, R. Duran, G. Rodriguez, J. Zheng, R. Zhang, D. Toom-Sauntry and W. R. Leaitch, Submicron organic aerosol in Tijuana, Mexico, from local and Southern California sources during the Calmex campaign, *Atmos. Environ.*, 2013, **70**, 500–512.

7 P. F. DeCarlo, J. R. Kimmel, A. Trimborn, M. J. Northway, J. T. Jayne, A. C. Aiken, M. Gonin, K. Fuhrer, T. Horvath, K. S. Docherty, D. R. Worsnop and J. L. Jimenez, Field-Deployable, High-Resolution, Time-of-Flight Aerosol Mass Spectrometer, *Anal. Chem.*, 2006, **78**, 8281–8289.

8 M. R. Canagaratna, J. T. Jayne, J. L. Jimenez, J. D. Allan, M. R. Alfarra, Q. Zhang, T. B. Onasch, F. Drewnick, H. Coe, A. Middlebrook, A. Delia, L. R. Williams, A. M. Trimborn, M. J. Northway, P. F. DeCarlo, C. E. Kolb, P. Davidovits and D. R. Worsnop, *Mass Spectrom. Rev.*, 2007, **26**, 185–222.

9 Q. Zhang, J. L. Jimenez, D. R. Worsnop and M. R. Canagaratna, A case study of urban particle acidity and its influence on secondary organic aerosol, *Environ. Sci. Technol.*, 2007, **41**, 3213–3219.

10 V. A. Lanz, A. S. H. Pŕevôt, M. R. Alfarra, S. Weimer, C. Mohr, P. F. DeCarlo, M. F. D. Gianini, C. Hueglin, J. Schneider, O. Favez, B. D'Anna, C. George and U. Baltensperger, Characterization of aerosol chemical composition with aerosol mass spectrometry in Central Europe: An overview, *Atmos. Chem. Phys.*, 2010, **10**, 10453–10471.

11 C. L. Martin, J. D. Allan, J. Crosier, T. W. Choularton, H. Coe and M. W. Gallagher, Seasonal variation of fine particulate composition in the centre of a UK city, *Atmos. Environ.*, 2011, **45**, 4379–4389.

12 J. Park, S. Lee, M. Kang, H. joo Cho, K. Lee and K. Park, Seasonal characteristics of submicrometer organic aerosols in urban Gwangju, Korea using an aerosol mass spectrometer, *Atmos. Environ.*, 2013, **80**, 445–454.

13 W. Hu, M. Hu, W. Hu, J. L. Jimenez, B. Yuan, W. Chen, M. Wang, Y. Wu, C. Chen, Z. Wang, J. Peng, L. Zeng and M. Shao, Chemical composition, sources, and aging process of submicron aerosols in Beijing: Contrast between summer and winter, *J. Geophys. Res.*, 2016, **121**, 1955–1977.

14 A. M. Johnson, M. S. Waring and P. F. DeCarlo, Real-time transformation of outdoor aerosol components upon transport indoors measured with aerosol mass spectrometry, *Indoor Air*, 2017, **27**, 230–240.

15 P. F. DeCarlo, A. M. Avery and M. S. Waring, Thirdhand smoke uptake to aerosol particles in the indoor environment, *Sci. Adv.*, 2018, **4**, 1–8.

16 Q. Y. Meng, B. J. Turpin, H. L. Jong, A. Polidori, C. P. Weisel, M. Morandi, S. Colome, J. Zhang, T. Stock and A. Winer, How does infiltration behavior modify the composition of ambient PM 2.5 in indoor spaces? An analysis of RIOPA data, *Environ. Sci. Technol.*, 2007, **41**, 7315–7321.

17 D. L. Liu and W. W. Nazaroff, Particle penetration through building cracks, *Aerosol Sci. Technol.*, 2003, **37**, 565–573.

18 W. J. Riley, T. E. McKone, A. C. K. Lai and W. W. Nazaroff, Indoor particulate matter of outdoor origin: Importance of size-dependent removal mechanisms, *Environ. Sci. Technol.*, 2002, **36**, 200–207.

19 L. A. Wallace, S. J. Emmerich and C. Howard-Reed, Source Strengths of Ultrafine and Fine Particles Due to Cooking with a Gas Stove, *Environ. Sci. Technol.*, 2004, **38**, 2304–2311.

20 W. W. Nazaroff and C. J. Weschler, Cleaning products and air fresheners: Exposure to primary and secondary air pollutants, *Atmos. Environ.*, 2004, **38**, 2841–2865.

21 B. C. Singer, H. Destaillats, A. T. Hodgson and W. W. Nazaroff, Cleaning products and air fresheners: Emissions and resulting concentrations of glycol ethers and terpenoids, *Indoor Air*, 2006, **16**, 179–191.

22 N. E. Klepeis, M. G. Apte, L. A. Gundel, R. G. Sextro and W. W. Nazaroff, Determining Size-Specific Emission Factors for Environmental Tobacco Smoke Particles, *Aerosol Sci. Technol.*, 2003, **37**, 780–790.

23 C. Chen and B. Zhao, Review of relationship between indoor and outdoor particles: I/O ratio, infiltration factor and penetration factor, *Atmos. Environ.*, 2011, **45**, 275–288.

24 C. D. Cappa and J. L. Jimenez, Quantitative estimates of the volatility of ambient organic aerosol, *Atmos. Chem. Phys.*, 2010, **10**, 5409–5424.

25 K. R. Kolesar, Z. Li, K. R. Wilson and C. D. Cappa, Heating-Induced Evaporation of Nine Different Secondary Organic Aerosol Types, *Environ. Sci. Technol.*, 2015, **49**, 12242–12252.

26 J. A. Huffman, K. S. Docherty, A. C. Aiken, M. J. Cubison, I. M. Ulbrich, P. F. DeCarlo, D. Sueper, J. T. Jayne, D. R. Worsnop, P. J. Ziemann and J. L. Jimenez, Chemically-resolved aerosol volatility measurements from two megacity field studies, *Atmos. Chem. Phys.*, 2009, **9**, 7161–7182.

27 N. M. Donahue, A. L. Robinson, C. O. Stanier and S. N. Pandis, Coupled partitioning, dilution, and chemical aging of semivolatile organics, *Environ. Sci. Technol.*, 2006, **40**, 2635–2643.

28 N. Hodas and B. J. Turpin, Shifts in the gas-particle partitioning of ambient organics with transport into the indoor environment, *Aerosol Sci. Technol.*, 2014, **48**, 271–281.

29 M. S. Waring, Secondary organic aerosol in residences: Predicting its fraction of fine particle mass and determinants of formation strength, *Indoor Air*, 2014, **24**, 376–389.

30 S. Duncan, K. G. Sexton and B. Turpin, Oxygenated VOCs, aqueous chemistry, and potential impacts on residential indoor air composition, *Indoor Air*, 2018, **28**, 198–212.

31 Z. Meng, J. H. Seinfeld, P. Saxena and Y. P. Kim, Contribution of Water to Particulate Mass in the South Coast Air Basin, *Aerosol Sci. Technol.*, 1995, **22**, 111–123.

32 B. Ervens, B. J. Turpin and R. J. Weber, Secondary organic aerosol formation in cloud droplets and aqueous particles (aqSOA): A review of laboratory, field and model studies, *Atmos. Chem. Phys.*, 2011, **11**, 11069–11102.
33 J. F. Pankow, Organic particulate material levels in the atmosphere: Conditions favoring sensitivity to varying relative humidity and temperature, *Proc. Natl. Acad. Sci.*, 2010, **107**, 6682–6686.
34 M. Shiraiwa, M. Ammann, T. Koop and U. Poschl, Gas uptake and chemical aging of semisolid organic aerosol particles, *Proc. Natl. Acad. Sci.*, 2011, **108**, 11003–11008.
35 N. Hodas, A. P. Sullivan, K. Skog, F. N. Keutsch, J. L. Collett, S. Decesari, M. C. Facchini, A. G. Carlton, A. Laaksonen and B. J. Turpin, Aerosol liquid water driven by anthropogenic nitrate: Implications for lifetimes of water-soluble organic gases and potential for secondary organic aerosol formation, *Environ. Sci. Technol.*, 2014, **48**, 11127–11136.
36 T. K. V Nguyen, M. D. Petters, S. R. Suda, H. Guo, R. J. Weber and A. G. Carlton, Trends in particle-phase liquid water during the Southern Oxidant and Aerosol Study, *Atmos. Chem. Phys.*, 2014, **14**, 10911–10930.
37 W. Xu, T. Han, W. Du, Q. Wang, C. Chen, J. Zhao, Y. Zhang, J. Li, P. Fu, Z. Wang, D. R. Worsnop and Y. Sun, Effects of aqueous-phase and photochemical processing on secondary organic aerosol formation and evolution in Beijing, China, *Environ. Sci. Technol.*, 2017, **51**, 762–770.
38 B. Jing, S. Tong, Q. Liu, K. Li, W. Wang, Y. Zhang and M. Ge, Hygroscopic behavior of multicomponent organic aerosols and their internal mixtures with ammonium sulfate, *Atmos. Chem. Phys.*, 2016, **16**, 4101–4118.
39 M. L. Pöhlker, C. Pöhlker, F. Ditas, T. Klimach, I. H. De Angelis, A. Araújo, J. Brito, S. Carbone, Y. Cheng, X. Chi, R. Ditz, S. S. Gunthe, J. Kesselmeier, T. Könemann, J. V. Lavrič, S. T. Martin, E. Mikhailov, D. Moran-Zuloaga, D. Rose, J. Saturno, H. Su, R. Thalman, D. Walter, J. Wang, S. Wolff, H. M. J. Barbosa, P. Artaxo, M. O. Andreae and U. Pöschl, Long-term observations of cloud condensation nuclei in the Amazon rain forest - Part 1: Aerosol size distribution, hygroscopicity, and new model parametrizations for CCN prediction, *Atmos. Chem. Phys.*, 2016, **16**, 15709–15740.
40 J. Duplissy, P. F. De Carlo, J. Dommen, M. R. Alfarra, A. Metzger, I. Barmpadimos, A. S. H. Prevot, E. Weingartner, T. Tritscher, M. Gysel, A. C. Aiken, J. L. Jimenez, M. R. Canagaratna, D. R. Worsnop, D. R. Collins, J. Tomlinson and U. Baltensperger, Relating hygroscopicity and composition of organic aerosol particulate matter, *Atmos. Chem. Phys.*, 2011, **11**, 1155–1165.
41 E. Swietlicki, H. C. Hansson, K. Hämeri, B. Svenningsson, A. Massling, G. Mcfiggans, P. H. Mcmurry, T. Petäjä, P. Tunved, M. Gysel, D. Topping, E. Weingartner, U. Baltensperger, J. Rissler, A. Wiedensohler and M. Kulmala, Hygroscopic properties of submicrometer atmospheric aerosol particles measured with H-TDMA instruments in various environments - A review, *Tellus, Ser. B: Chem. Phys. Meteorol.*, 2008, **60**, 432–469.
42 N. K. Meyer, J. Duplissy, M. Gysel, A. Metzger, J. Dommen, E. Weingartner, M. R. Alfarra, A. S. H. Prevot, C. Fletcher, N. Good, G. Mcfiggans, A. M. Jonsson, M. Hallquist, U. Baltensperger and Z. D. Ristovski, Analysis of the hygroscopic and volatile properties of ammonium sulphate seeded and unseeded SOA particles, *Atmos. Chem. Phys.*, 2009, **9**, 721–732.
43 A. M. Middlebrook, R. Bahreini, J. L. Jimenez and M. R. Canagaratna, Evaluation of composition-dependent collection efficiencies for the Aerodyne aerosol mass spectrometer using field data, *Aerosol Sci. Technol.*, 2012, **46**(3), 258–271.
44 N. Takegawa, Y. Miyazaki, Y. Kondo, Y. Komazaki, T. Miyakawa, J. L. Jimenez, J. T. Jayne, D. R. Worsnop, J. D. Allan and R. J. Weber, Characterization of an Aerodyne Aerosol Mass Spectrometer (AMS): Intercomparison with Other Aerosol Instruments, *Aerodyne Aerosol Mass Spectrometer*, 2005, **39**, 760–770.
45 J. D. Allan, A. E. Delia, H. Coe, K. N. Bower, M. R. Alfarra, J. L. Jimenez, A. M. Middlebrook, F. Drewnick, T. B. Onasch, M. R. Canagaratna, J. T. Jayne and D. R. Worsnop, A generalised method for the extraction of chemically resolved mass spectra from Aerodyne aerosol mass spectrometer data, *J. Aerosol Sci.*, 2004, **35**, 909–922.
46 A. C. Aiken, P. F. DeCarlo, J. H. Kroll, D. R. Worsnop, J. A. Huffman, K. S. Docherty, I. M. Ulbrich, C. Mohr, J. R. Kimmel, D. Sueper, Y. Sun, Q. Zhang, A. Trimborn, M. Northway, P. J. Ziemann, M. R. Canagaratna, T. B. Onasch, M. R. Alfarra, A. S. H. Prevot, J. Dommen, J. Duplissy, A. Metzger, U. Baltensperger and J. L. Jimenez, O/C and OM/OC ratios of primary, secondary, and ambient organic aerosols with high-resolution time-of-flight aerosol mass spectrometry, *Environ. Sci. Technol.*, 2008, **42**, 4478–4485.
47 M. R. Canagaratna, J. L. Jimenez, J. H. Kroll, Q. Chen, S. H. Kessler, P. Massoli, L. Hildebrandt Ruiz, E. Fortner, L. R. Williams, K. R. Wilson, J. D. Surratt, N. M. Donahue, J. T. Jayne and D. R. Worsnop, Elemental ratio measurements of organic compounds using aerosol mass spectrometry: Characterization, improved calibration, and implications, *Atmos. Chem. Phys.*, 2015, **15**, 253–272.
48 L. Drinovec, G. Močnik, P. Zotter, A. S. H. Prévôt, C. Ruckstuhl, E. Coz, M. Rupakheti, J. Sciare, T. Müller, A. Wiedensohler and A. D. A. Hansen, The 'dual-spot' Aethalometer: An improved measurement of aerosol black carbon with real-time loading compensation, *Atmos. Meas. Tech.*, 2015, **8**, 1965–1979.
49 D. K. Farmer, A. Matsunaga, K. S. Docherty, J. D. Surratt, J. H. Seinfeld, P. J. Ziemann and J. L. Jimenez, Response of an aerosol mass spectrometer to organonitrates and organosulfates and implications for atmospheric chemistry, *Proc. Natl. Acad. Sci.*, 2010, **107**, 6670–6675.
50 A. Kiendler-Scharr, A. A. Mensah, E. Friese, D. Topping, E. Nemitz, A. S. H. Prevot, M. Äijälä, J. Allan, F. Canonaco, M. R. Canagaratna, S. Carbone, M. Crippa, M. Dall Osto, D. A. Day, P. De Carlo, C. F. Di Marco, H. Elbern, A. Eriksson, E. Freney, L. Hao, H. Herrmann,

L. Hildebrandt, R. Hillamo, J. L. Jimenez, A. Laaksonen, G. McFiggans, C. Mohr, C. O'Dowd, R. Otjes, J. Ovadnevaite, S. N. Pandis, L. Poulain, P. Schlag, K. Sellegri, E. Swietlicki, P. Tiitta, A. Vermeulen, A. Wahner, D. Worsnop and H. C. Wu, Ubiquity of organic nitrates from nighttime chemistry in the European submicron aerosol, *Geophys. Res. Lett.*, 2016, **43**, 7735–7744.

51 P. Paatero and U. Tapper, Positive Matrix Factorization: A non-negative factor model with optimal utilization of erro estimates of data values, *Environmetrics*, 1994, **5**, 111–126.

52 V. A. Lanz, M. R. Alfarra, U. Baltensperger, B. Buchmann, C. Hueglin and A. S. H. Prévôt, Source apportionment of submicron organic aerosols at an urban site by factor analytical modelling of aerosol mass spectra, *Atmos. Chem. Phys.*, 2007, **7**, 1503–1522.

53 I. M. Ulbrich, M. R. Canagaratna, Q. Zhang, D. R. Worsnop and J. L. Jimenez, Interpretation of organic components from Positive Matrix Factorization of aerosol mass spectrometric data, *Atmos. Chem. Phys.*, 2009, **9**, 2891–2918.

54 M. D. Petters and S. M. Kreidenweis, A single parameter representation of hygroscopic growth and cloud condensation nucleus activity, *Atmos. Chem. Phys.*, 2007, **7**, 1961–1971.

55 M. Gysel, J. Crosier, D. O. Topping, J. D. Whitehead, K. N. Bower, M. J. Cubison, P. I. Williams, M. J. Flynn, G. B. McFiggans and H. Coe, Closure study between chemical composition and hygroscopic growth of aerosol particles during TORCH2, *Atmos. Chem. Phys.*, 2007, **7**, 6131–6144.

56 C. Mohr, P. F. DeCarlo, M. F. Heringa, R. Chirico, J. G. Slowik, R. Richter, C. Reche, A. Alastuey, X. Querol, R. Seco, J. Peñuelas, J. L. Jimenez, M. Crippa, R. Zimmermann, U. Baltensperger and A. S. H. Prévôt, Identification and quantification of organic aerosol from cooking and other sources in Barcelona using aerosol mass spectrometer data, *Atmos. Chem. Phys.*, 2012, **12**, 1649–1665.

57 M. Crippa, I. El Haddad, J. G. Slowik, P. F. DeCarlo, C. Mohr, M. F. Heringa, R. Chirico, N. Marchand, J. Sciare, U. Baltensperger and A. S. H. Prévôt, Identification of marine and continental aerosol sources in Paris using high resolution aerosol mass spectrometry, *J. Geophys. Res.: Atmos.*, 2013, **118**, 1950–1963.

58 A. Setyan, Q. Zhang, M. Merkel, W. B. Knighton, Y. Sun, C. Song, J. E. Shilling, T. B. Onasch, S. C. Herndon, D. R. Worsnop, J. D. Fast, R. A. Zaveri, L. K. Berg, A. Wiedensohler, B. A. Flowers, M. K. Dubey and R. Subramanian, Characterization of submicron particles influenced by mixed biogenic and anthropogenic emissions using high-resolution aerosol mass spectrometry: results from CARES, *Atmos. Chem. Phys.*, 2012, **12**, 8131–8156.

59 Q. Zhang, M. Rami Alfarra, D. R. Worsnop, J. D. Allan, H. Coe, M. R. Canagaratna and J. L. Jimenez, Deconvolution and quantification of hydrocarbon-like and oxygenated organic aerosols based on aerosol mass spectrometry, *Environ. Sci. Technol.*, 2005, **39**, 4938–4952.

60 M. R. Canagaratna, J. T. Jayne, D. A. Ghertner, S. Herndon, Q. Shi, J. L. Jimenez, P. J. Silva, P. Williams, T. Lanni, F. Drewnick, K. L. Demerjian, C. E. Kolb and D. R. Worsnop, Chase Studies of Particulate Emissions from in-use New York City Vehicles, *Aerosol Sci. Technol.*, 2004, **38**, 555–573.

61 M. Crippa, P. F. DeCarlo, J. G. Slowik, C. Mohr, M. F. Heringa, R. Chirico, L. Poulain, F. Freutel, J. Sciare, J. Cozic, C. F. Di Marco, M. Elsasser, J. B. Nicolas, N. Marchand, E. Abidi, A. Wiedensohler, F. Drewnick, J. Schneider, S. Borrmann, E. Nemitz, R. Zimmermann, J. L. Jaffrezo, A. S. H. Prévôt and U. Baltensperger, Wintertime aerosol chemical composition and source apportionment of the organic fraction in the metropolitan area of Paris, *Atmos. Chem. Phys.*, 2013, **13**, 961–981.

62 F. Freutel, F. Drewnick, J. Schneider, T. Klimach and S. Borrmann, Quantitative single-particle analysis with the Aerodyne aerosol mass spectrometer: Development of a new classification algorithm and its application to field data, *Atmos. Meas. Tech.*, 2013, **6**, 3131–3145.

63 J. L. Jimenez, M. R. Canagaratna, N. M. Donahue, A. S. H. Prevot, Q. Zhang, J. H. Kroll, P. F. DeCarlo, J. D. Allan, H. Coe, N. L. Ng, A. C. Aiken, K. S. Docherty, I. M. Ulbrich, A. P. Grieshop, A. L. Robinson, J. Duplissy, J. D. Smith, K. R. Wilson, V. A. Lanz, C. Hueglin, Y. L. Sun, J. Tian, A. Laaksonen, T. Raatikainen, J. Rautiainen, P. Vaattovaara, M. Ehn, M. Kulmala, J. M. Tomlinson, D. R. Collins, M. J. Cubison, E. J. Dunlea, J. A. Huffman, T. B. Onasch, M. R. Alfarra, P. I. Williams, K. Bower, Y. Kondo, J. Schneider, F. Drewnick, S. Borrmann, S. Weimer, K. Demerjian, D. Salcedo, L. Cottrell, R. Griffin, A. Takami, T. Miyoshi, S. Hatakeyama, A. Shimono, J. Y. Sun, Y. M. Zhang, K. Dzepina, J. R. Kimmel, D. Sueper, J. T. Jayne, S. C. Herndon, A. M. Trimborn, L. R. Williams, E. C. Wood, A. M. Middlebrook, C. E. Kolb, U. Baltensperger and D. R. Worsnop, Evolution of organic aerosols in the atmosphere, *Science*, 2009, **326**, 1525–1529.

64 E. C. Wood, M. R. Canagaratna, S. C. Herndon, T. B. Onasch, C. E. Kolb, D. R. Worsnop, J. H. Kroll, W. B. Knighton, R. Seila, M. Zavala, L. T. Molina, P. F. DeCarlo, J. L. Jimenez, A. J. Weinheimer, D. J. Knapp, B. T. Jobson, J. Stutz, W. C. Kuster and E. J. Williams, Investigation of the correlation between odd oxygen and secondary organic aerosol in Mexico City and Houston, *Atmos. Chem. Phys.*, 2010, **10**, 8947–8968.

65 R. Chirico, A. S. H. Prevot, P. F. DeCarlo, M. F. Heringa, R. Richter, E. Weingartner and U. Baltensperger, Aerosol and trace gas vehicle emission factors measured in a tunnel using an Aerosol Mass Spectrometer and other on-line instrumentation, *Atmos. Environ.*, 2011, **45**, 1282–2192.

66 C. J. Weschler and H. C. Shields, Experiments probing the influence of air exchange rates on secondary organic aerosols derived from indoor chemistry, *Atmos. Environ.*, 2003, **37**, 5621–5631.

67 M. S. Waring and J. A. Siegel, Indoor secondary organic aerosol formation initiated from reactions between ozone

and surface-sorbed d -limonene, *Environ. Sci. Technol.*, 2013, **47**, 6341–6348.

68 D. Rim, J. Il Choi and L. A. Wallace, Size-Resolved Source Emission Rates of Indoor Ultrafine Particles Considering Coagulation, *Environ. Sci. Technol.*, 2016, **50**, 10031–10038.

69 J. Rissler, E. Z. Nordin, A. C. Eriksson, P. T. Nilsson, M. Frosch, M. K. Sporre, A. Wierzbicka, B. Svenningsson, J. Löndahl, M. E. Messing, S. Sjogren, J. G. Hemmingsen, S. Loft, J. H. Pagels and E. Swietlicki, Effective density and mixing state of aerosol particles in a near-traffic urban environment, *Environ. Sci. Technol.*, 2014, **48**, 6300–6308.

70 P. F. DeCarlo, J. G. Slowik, D. R. Worsnop, P. Davidovits and J. L. Jimenez, Particle Morphology and Density Characterization by Combined Mobility and Aerodynamic Diameter Measurements. Part 1: Theory, *Aerosol Sci. Technol.*, 2004, **38**, 1185–1205.

71 P. Massoli, E. C. Fortner, M. R. Canagaratna, L. R. Williams, Q. Zhang, Y. Sun, J. J. Schwab, A. Trimborn, T. B. Onasch, K. L. Demerjian, C. E. Kolb, D. R. Worsnop and J. T. Jayne, Pollution gradients and chemical characterization of particulatematter from vehicular traffic near major roadways: Results from the 2009 queens college air quality study in NYC, *Aerosol Sci. Technol.*, 2012, **46**, 1201–1218.

72 T. Tritscher, Z. Jurnyi, M. Martin, R. Chirico, M. Gysel, M. F. Heringa, P. F. DeCarlo, B. Sierau, A. S. H. Prévt, E. Weingartner and U. Baltensperger, Changes of hygroscopicity and morphology during ageing of diesel soot, *Environ. Res. Lett.*, 2011, **6**, 1–10.

73 A. G. Carlton and B. J. Turpin, Particle partitioning potential of organic compounds is highest in the Eastern US and driven by anthropogenic water, *Atmos. Chem. Phys.*, 2013, **13**, 10203–10214.

74 M. M. H. El-Sayed, Y. Wang and C. J. Hennigan, Direct atmospheric evidence for the irreversible formation of aqueous secondary organic aerosol, *Geophys. Res. Lett.*, 2015, **42**, 5577–5586.

75 M. M. H. El-Sayed, D. Amenumey and C. J. Hennigan, Drying-Induced Evaporation of Secondary Organic Aerosol during Summer, *Environ. Sci. Technol.*, 2016, **50**, 3626–3633.

76 S. Youssefi and M. S. Waring, Indoor transient SOA formation from ozone+α-pinene reactions: Impacts of air exchange and initial product concentrations, and comparison to limonene ozonolysis, *Atmos. Environ.*, 2015, **112**, 106–115.

77 X. Chen and P. K. Hopke, A chamber study of secondary organic aerosol formation by limonene ozonolysis, *Indoor Air*, 2010, **20**, 320–328.

78 Å. M. Jonsson, M. Hallquist and E. Ljungström, Impact of humidity on the ozone initiated oxidation of limonene, Δ3-carene, and α-pinene, *Environ. Sci. Technol.*, 2006, **40**, 188–194.